UNDERSTANDING THE DEPOSITION OF MG AND INTERCALATION OF MG^{2+} FOR FUTURE MG-ION BATTERIES

BY

ELIZABETH CAROL MILLER

THESIS

Submitted in partial fulfillment of the requirements
for the degree of Master of Science in Chemistry
in the Graduate College of the
University of Illinois at Urbana-Champaign, 2015

Urbana, Illinois

Adviser:

Professor Andrew Gewirth

ABSTRACT

In efforts to decrease the world's dependence on fossil fuels, renewable energy sources and storage are being actively sought, especially in the transportation sector. The electrification of vehicles hinges on the low cost, safety, and volumetric capacity of its energy storage devices, namely batteries. Currently, Li-ion batteries are used in commercial electric vehicles; however, these have limited capacities compared to metal anode batteries. Herein, this work describes the methods and advancements in understanding and developing Mg batteries, as an alternative to Li-ion batteries. Theoretically, Mg batteries have far superior volumetric capacities (3833 $mAhcm^{-3}$ Mg vs. 760 $mAhcm^{-3}$ graphite). Mg is a more earth abundant (13.9% Mg in earth's crust compared to $7x10^{-4}$ % Li) and a less expensive alternative to Li ($2700/ton Mg and $64000/ton Li).

In Chapter 1, polyoxometalates are electrochemically characterized as a possible cathode material for Mg-ion batteries. Phosphomolybdic acid is used a proof of concept material, showing reversible redox chemistry in a variety of nonaqueous electrolyte systems. Efforts are described to reduce dissolution with polymer binders and how the redox chemistry changes with cationic salts.

In Chapter 2, the electrochemistry of Mg deposition and dissolution from the magnesium aluminum chloride complex is described. The results define the requirements for reversible behavior with ~100% Coulombic efficiencies. Voltammetric cycling alters the composition and the performance of the electrolyte. The electrolyte has no shelf life, and oligomers form due to the ring-opening polymerization of the THF solvent. From these results, a mechanism is proposed describing how the conditioning process of the MACC in THF improves its performance by both tuning the Mg:Al stoichiometry and eliminating oligomers.

To Chris and my Dad,
who showed me how to pursue God's love and truth
through the study of chemistry

Nie można bowiem mieć nadziei na skierowanie świata ku lepszym drogom, o ile się jednostek nie skieruje ku lepszemu.

W tym celu każdy z nas powinien pracować nad udoskonaleniem się własnym, jednocześnie zdając sobie sprawę ze swej, osobistej odpowiedzialności za całokształt tego, co się dzieje w świecie

You cannot hope to build a better world without improving the individuals.

To that end, each of us must work for our own improvement while being aware of our personal responsibility for the whole of what is happening in the world

Maria Skłodowska-Curie

ACKNOWLEDGMENTS

My time and success in graduate school is largely founded on the support and encouragement of the people I have met along the way. Each person in their own way has left a lasting impression on me, and I hope to do the same as I pursue a future in teaching chemistry.

In the classroom and in the lab, several professors have left lasting impressions. I would like to thank Professors Gwenda Schmidt-Snoek and Andy Gewirth for mentoring me in my research. Under their guidance at Hope College and at the University of Illinois at Urbana-Champaign, I learned how to develop experiments, write papers, and share my knowledge with the greater scientific community. They are both shining examples of how to motivate students in their research groups, and I am grateful to be among their students. I have also been blessed by the mentorship of instructors, whose teaching abilities I hold in the highest regard: Beth Warren, David Brothers, Konni Russek, Beth Anderson, William Polik, and Christian Ray. I have been transformed by the discussions and classes with this great cloud of chemists and instructors, and they deserve my sincerest thanks.

I have been profoundly influenced by the support of friends and peers, and I would like to acknowledge them. I am indebted to the women of Hope College for their encouragement over the years. I have had the pleasure to work with brilliant scholars from around the world: Edmund Tse, Hengliang Wu, Jason Varnell, Yeyoung Ha, Bruno Nicolau, Jinho Chang, and Kevin Schmitt to name a few. I am especially grateful to Brittany Walker, Brian Trinh, Xiling Zhao, Eva Czarniecki, and Ricardo Venegas for their support and friendship. I highly esteem these scientists and truly wish the very best in the careers and in life.

My family has been very supportive of me and deserves praise. Growing up to my father's favorite mantra "graph paper is our friend" – I am not surprised by the curiosity and

contagious enthusiasm shared by my family. My brothers inspire me by the depth of their passions. I am blessed to have such encouraging brothers as Alex and Patrick. My dad, more than anyone else, has built up a love for science in me. From my earliest memories, I knew I wanted to be like him – little did I know that I would become a chemist, too. I would like to acknowledge my biggest role model, my mom, whose fearlessness throughout her life motivates me to always improve, to love graciously, and to use my skills and knowledge for the betterment of others.

Finally, I would like to thank Chris. I cannot imagine my time in graduate school or my future without him. Of all the takeaways from this place – increased wisdom, high impact publications, a few acid burns – I never dreamed that I would find what most people spend their whole lives seeking – a best friend and true love. I am inspired daily by his wisdom in all things, his ability to motivate others, his humility, his love for his family, and his pursuit of God's truth. Without Chris I could have never come this far, and I am eternally grateful for him.

To all these people named and unnamed, I give my sincerest thanks.

TABLE OF CONTENTS

CHAPTER 1: Polyoxometalates as Cathode Materials for Mg-ion Batteries 1

1.1 INTRODUCTION 1

1.2 EXPERIMENTAL 10

1.3 RESULTS AND DISCUSSION 14

1.4 CONCLUSIONS 23

1.5 REFERENCES 24

CHAPTER 2: Electrochemical Insight into Mg Deposition and Dissolution Pathways 30

2.1 INTRODUCTION 30

2.2 EXPERIMENTAL DETAILS 32

2.3 RESULTS AND DISCUSSION 35

2.4 CONCLUSIONS 61

2.5 REFERENCES 62

CHAPTER 1: Polyoxometalates as Cathode Materials for Mg-ion Batteries

1.1 INTRODUCTION

In 2011, petroleum accounted for one third of the world's energy use.[1] With CO_2 levels rising above 400 ppm, widespread efforts are being researched and implemented to address sustainable energy sources.[2] As countries transition from coal and nuclear power sources to cleaner, safer, renewable resources like wind and solar, energy storage is central.[3] Many renewable energy sources are intermittent and require storage for energy consumption during all periods of the day.

Batteries, fuel cells, and pumped hydro-electric all provide means of energy storage. However, no single storage solution addresses all possible applications. For example, portable devices like cell phones and laptops cannot use pumped-hydro for energy storage. Instead pumped-hydro is better suited to stationary and grid storage.[4] The energy storage systems for the grid are not necessarily the same as those for electric vehicles. In electric vehicles, volumetric capacity and safety are highly valued for energy storage devices.

1.1.1 LI-ION BATTERIES AND ELECTRIC VEHICLES

Both batteries and fuel cells have been researched as a replacement for gasoline in commercial vehicles, and a growing number of electric and hybrid-electric vehicles exist on today's market.[5] Fuel cells often use compressed and flammable gases, which pose safety concerns.[6] Additionally the best catalyst for fuel cells is Pt, which would need to be replaced by cheaper catalysts for fuel cells to be a viable option for vehicle commercialization.[7,8] Therefore, battery technologies are highly sought to replace gasoline in vehicles. Many hybrid vehicles use nickel metal-hydride batteries while electric vehicles like the Tesla Model S, Chevy Volt, and Nissan Leaf use Li-ion batteries. Although less dependent on fossil fuels directly, the cost and

environmental impact of producing electric vehicles still needs significant improvement.[9] Of importance, Li-ion batteries cannot use Li metal as the anode due to dendrite formation.[10] To mitigate this problem, lower capacity anodes like graphite must be used to intercalate Li ions. Graphite electrodes are a safe option; however the volumetric capacity of the battery is sacrificed. For these reasons, metal anode batteries with high capacities need to be investigated.

1.1.2 MAGNESIUM BATTERIES

Mg batteries have the potential to revolutionize energy storage as an alternative to Li-ion batteries. Theoretically these batteries far outperform current Li-ion batteries in both volumetric and gravimetric capacities (Table 1).[11] Additionally, Mg is a more earth abundant (13.9% Mg in earth's crust compared to $7x10^{-4}$ % Li) and a less expensive alternative ($2700/ton Mg and $64000/ton Li). Much of the excitement over Mg batteries stems from the possibility of using a Mg metal anode. While early work in the 1990s paved the way for Mg battery research, the research by Aurbach and co-authors catalyzed this interest over the past 15 years.[12,13] They showed full battery studies using a Mg metal anode, Chevrel Mo_6S_8 cathode in Grignard-type electrolytes. Since then, all aspects of the battery have improved and are more widely understood.[14]

Table 1.1: Theoretical capacities of graphite (LiC_6) and Mg metal.[11]

Anode Material	**Volumetric Capacity ($mAhcm^{-3}$)**	**Gravimetric Capacity ($mAhg^{-1}$)**
Graphite	760	372
Mg	3833	2205

Despite the attractive properties of Mg batteries, their implementation has been hindered by several challenges[15], including:

1) Electrolyte reactivity and nontrivial deposition
2) Reversibility and kinetics of Mg^{2+} intercalation into cathodes

3) Electrolyte compatibility with electrodes

Conventional solvent-salt analogs of Li-ion battery electrolytes (carbonates with salts) do not show reversible Mg deposition.[16] Unlike Li deposition which forms as ion permeable solid electrolyte interface, passivating films form in these simple salt solvents for Mg. Although the mechanism is not well understood, the solvation and deposition of Mg is more complicated than in Li systems.[17] Electrolytes have progressed from reactive Grignard reagents to organo-haloaluminate electrolytes.[18,19] Due to the organic components of these electrolytes, they are reactive and have limited electrochemical voltage windows. Recently, an electrolyte formed from $MgCl_2$ and $AlCl_3$, which contains an entirely inorganic complex (MACC) in ether solvents, has demonstrated ~100% Coulombic efficiency for Mg deposition and stripping with a voltage window up to 3 V vs. Mg.[20,21] This window would allow higher voltage materials to be tested as potential cathodes. Unfortunately, the stability and reactivity of this electrolyte to impurities and cathode materials make testing difficult.[22]

As a work around, possible cathodes are frequently tested in electrolytes that do not support reversible Mg deposition, like perchlorates in CH_3CN.[23] Studies by Novak et al. have shown that the dryness of the solvent is important for voltammetry in sulfides and oxides.[24] Using these electrolytes, Mg^{2+} intercalation can be probed for various materials. However, these studies are limited to half cell experiments, and full cell studies cannot be performed, where two electrodes are used in a coin cell to interrogate the charge and discharge profiles of the battery. It is therefore important to understand the mechanism of Mg deposition and to tailor electrolytes to be less reactive and have high stability with good reversibility, shown in Chapter 2. Studies also should focus on understanding the intercalation processes of Mg cations into cathode materials, explored in Chapter 1.

1.1.3 BACKGROUND AND INSPIRATION

Multivalent batteries have been increasingly studied in the past 15 years. As an alternative to Li-ion batteries, it is important for multivalent batteries to have similar or better metrics of performance including: high voltage, high volumetric and/or gravimetric capacity, high reversibility, low cost, low weight, and low volume. Several examples in literature have inspired this work and are used as a point of comparison to the materials presented later.

1.1.4 LITERATURE REVIEW

Several materials and material classes have been proposed as potential cathodes for the commercialization of Mg-ion batteries. As with electrolytes, analogs from Li-ion batteries have been attempted with marginal success. Both conversion and intercalation cathodes have been studied.

1.1.5 CHEVREL

The only successful full Mg battery prototypes have used Chevrel phase cathodes, Mo_6S_8, and its derivatives.[13,25] These cathodes incorporate a delocalized framework to accommodate the charge and diffusion of Mg^{2+} ions. The multiple Mo ions allow for a diffuse charge network to accommodate intercalated Mg^{2+} ions. These cathodes were the first to show reversible Mg^{2+} intercalation in electrolytes known to reversibly deposit Mg. Chevrel is often used as a benchmark to show the potential of new electrolytes and as means as a comparison to novel cathode materials. However, Chevrel phase cathodes suffer from low voltages (~1.1 V vs. Mg/Mg^{2+}) and only partial reversibility, where the total capacity drops by ~40% after the first discharge cycle.[15] Several groups have worked to improve the voltage through nanoparticles and by understanding the impact of Cu impurities.[26,27]

1.1.6 OTHER CATHODES

MgS

Magnesium sulfide has also been considered as a possible cathode material. Due to a rise in lithium sulfur battery research, a magnesium analog could be promising as well.[28,29] With theoretical specific and volumetric energy densities of 804 Wh/kg and 2597 Wh/L respectively, MgS batteries have potential as a future battery.[30] However, MgS batteries have not been widely investigated largely because MgS is nontrivial to synthesize, as MgO forms readily.[31,32] In 2011 Muldoon et al. showed a proof of concept for a rechargeable Mg-S battery.[33] The capacity quickly faded, due to dissolution of sulfur and polysulfides, and since this report, no follow-up studies have been shown.

V_2O_5

V_2O_5 has been shown to incorporate Mg ions in the presence of water.[24] Studies suggest that the solvated Mg-ion can be inserted in the bulk structure of the bronze with capacities around 150 mAh/g.[34] Various aerogels and nanotubular structures have been used to improve the sluggish kinetics and increases in performance are attributed to the shorter diffusion path.[35,36]

MnO_2

MnO_2 has been studied for several years as a potential cathode for Mg-ion batteries. With promising capacities, MnO_2 has been investigated in both electrolyte systems that support reversible Mg deposition, as well as systems that do not. Unfortunately, these reports suggest that (like V_2O_5) Mg-ions only intercalate when solvated by water in CH_3CN or propylene carbonate (PC) electrolytes.[37,38] In Mg-hexamethyldisilazane (Mg-HDMS) in THF, X-ray studies demonstrated irreversible Mg intercalation during initial cycling.[23] Importantly, most studies do not show voltammetry of the MnO_2, and the ones that performed cyclic voltammetry do not

show any reversible redox features.[39] For these reasons, it is believed that capacities are from solvent decomposition or interactions with the carbon support and polymer binder.

$MgFeSiO_4$

With a voltage of 2.4 V vs. Mg/Mg^{2+} and a theoretical capacity of 300 mAh/g, $MgFeSiO_4$ is another candidate Mg cathode material.[40] Orikasa et al. have tested this material in $Mg(TFSI)_2$ in triglyme and in CH_3CN in full cell configurations. Through X-ray studies, they showed that the material changes during charging or discharging the battery. However, cyclic voltammetry of the cathode material in a half cell design was not shown. Because reversible voltammetry was not provided, it is possible that capacities are due to the decomposition of solvent and that X-ray changes are also a result of this decomposition.

Several more examples exist in the literature, and the reader is referred to the recent review by Saha et al. for a more detailed overview.[15]

1.1.7 POLYOXOMETALATES

Polyoxometalates (POMs) are a class of materials characterized by early transition metal clusters.[41] Several thousand molecules are considered POMs and follow the general formula $[MO_x]_n$, where M = Mo, W, V and Nb and x = 4-7.[42] POMs are generally divided into several classes; some of the more commonly studied classes include Keggin $[M_{12}O_{36}(XO_4)]^{n-}$, Wells-Dawson $[M_{18}O_{54}(XO_4)_2]^{n-}$, and Anderson $[M_6O_{20}(XO_4)]^{n-}$. Due to the variety of structures, these "building blocks" allow for a tailored approach to designing materials.[43] POMs have been shown to self assemble into a variety of structures including films, nanowires, micelles, and dots.[44,45]

POMs have a diverse set of physical and electrochemical properties, giving rise to a wide range of applications, including electrochromic devices,[46] electrochemical capacitors,[47] flash memory devices,[48] catalysis,[49,50] biomedical applications,[51] and battery cathodes.[52] Remarkably,

many POMs can undergo reversible redox chemistry without changing their structures.[43] Recent X-ray studies have shown that all 12 Mo^{6+} ions in phosphomolybdic acid $[PMo_{12}O_{40}]^{27-}$ (PMA) can undergo a 2-electron reduction to Mo^{4+} reversibly.[53] This finding suggests that 24 electrons can be stored in a single PMA molecule, giving rise to large capacity. Due to the high theoretical capacities and voltages, various POMs have been studied for use as battery cathodes.

For applications in cathode designs, confining the POMs to an electrode surface is important. Several studies have shown stable films of POMs using Langmuir-Blodgett (LB) films and layer-by-layer assembly.[54] Electrodeposition of POMs is another method of functionalizing electrodes. [46,55,56,54] However these methods may not be conductive enough for cathode applications or have enough active material (in the case of surface modification of electrodes).

To be a viable candidate for cathode materials, POM solubility must be addressed. The solubility of POMs like PMA in common solvents including H_2O, CH_3CN, THF, and PC hinders performance of the cathode and makes characterization difficult. To overcome this dissolution problem, polymer binders are often employed. One must confine the POM to the surface in such a way that allows the transport of charged species to and from the electrode and solution interface. Therefore, polymer binders with high cationic conductivity are chosen.

1.1.8 SOLID-STATE ELECTROLYTE REVIEW

Solid electrolyte studies for Mg-ion batteries have recently explored the conductivity of Mg through polymer gels. Sheha, et al. recently showed that the polymer electrolyte of poly (vinyl alcohol), succinonitrile, and phosophotungstic acid (a POM) with $MgBr_2$ had a relatively small capacity (17.5 mAh/g) and low conductivity (10^{-7} – 10^{-5} S/cm).[57] Sharma and Hashmi greatly increased the conductivity of Mg ($6*10^{-4}$ S/cm) in a system using 1:1 poly (ethylene

oxide) (PEO) with magnesium trifluoromethanesulfonate ($Mg(OTf)_2$) and 30% weight succinonitrile.[58] Agrawal and Sahu note that the Mg^{2+} conductivity of pure PEO is quite low ($3.2 * 10^{-9}$ S/cm) and that the addition of Mg salts and small amounts of oxides greatly increases this value (10^{-5} S/cm).[59] Several other groups have shown the use of polyaniline and PVDF as useful binders.[60,61] Since ionic conduction is more predictive of cathode performance than electronic conduction, it is important to distinguish between these and test these characteristics well.[62,63]

1.1.9 MAGNESIATED-POLYOXOMETALATES

Various polyoxometalates were considered as possible cathode materials for Mg batteries. Possible options include those with reversible redox chemistries at high potentials vs. Mg, theoretical capacities, and having the ability to incorporate Mg^{2+} into the material. Magnesiated-POMs would be an interesting option, where one could investigate the crystal changes before and after a discharge cycle. Mg-POMs are not commercially available, so synthetic routes were considered. Günter et al. crystallized magnesium heteropolytungstates in the late 1980s.[64] Their group later found the true stoichiometry to be $Mg_7(MgW_{12}O_{42})(OH)_4(H_2O)_8$, suggesting that Mg had different coordination sites in the lattice.[65] In 1997, Tatibouët et al. characterized a magnesiated-POM with a Keggin structure and formula of $HMgPMo_{12}O_{40}$.[66] Although attempted, for final tests these materials were not used, due to the difficulty in characterization and growing crystals.

1.1.10 POLYOXOMETALTES IN BATTERIES

Several studies have shown the promise of polyoxometalate clusters for use in batteries. Recently a flow battery with vanadium and tungsten polyoxometalates was demonstrated with high Coulombic efficiencies and stability.[67] More commonly, cathodes for Li-ion secondary

batteries have been investigated. POMs like $K_3[PMo_{12}O_{40}]$, $(C_4H_9)_4N_3[PMo_{12}O_{40}]$, and $Na_3[AlMo_6O_{24}H_6]$ reversibly intercalate Li-ions.[52,68,69] Work with $Na_3[AlMo_6O_{24}H_6]$, an Anderson type POM, used polytetrafluoroethylene (PTFE) as the polymer binder. Derivatives of the PMA have also been widely studied for the intercalation of Li-ions.[70] The Awaga group found that lower weight % of PMA in the cathode increased performance when using polyvinylidene fluoride (PVDF) as the polymer binder.[69,71] Paik et al. showed reversible intercalation into polyaniline-PMA nanowires.[70]

Our research took inspiration from these works, using PMA as the proof of concept material for Mg-ion batteries. We also modeled our cathode design and testing on these examples.

1.2 EXPERIMENTAL

All chemicals were purchased from Sigma-Aldrich unless otherwise stated.

1.2.1 PREPARATION OF CATHODES

PMA (SPI-Chem), carbon black (Super P, Timcal), and a polymer binder were mixed in various ratios for cathode studies (Table 2). These mixtures were pulverized for 10 minutes using a mortar and pestle. A slurry was made by suspending the mixture in 1-methyl-2-pyrroidinone (NMP) and was cast on various current collectors using a Gardco adjustable micrometer film applicator (Table 3) (Microm II, 5 1/2″ width). All reported cathodes are cast on Al unless stated otherwise. The cathodes were dried in an oven at 70 ºC for 30 minutes. The dried cathodes were had a diameter of 7/16 inch (11.1 mm) and had an average mass loading of 1 mg/cm^2.

Table 1.2: Polymer binders used in the preparation of cathodes.

Polymer Binder	**Abbreviation**	**Source**	**Weight Ratio PMA:Carbon:Binder**
Polyvinylidene fluoride	PVDF	Kynar 2801	40:40:20 1:1:1
Poly (ethylene oxide)	PEO	Sigma M_v 100000	40:40:20 1:1:1
Polyaniline	PANI	Sigma	40:40:20 1:1:1
Poly (4-vinylpyridine)	PVP	Aldrich M_w 60000	40:40:20 1:1:1
Polytetrafluoroethylene	PTFE	Sigma	40:40:20 1:1:1

Table 1.3: Current collectors used in preparation of cathodes.

Current Collector	**Source**
Aluminum Foil	Sigma Aldrich
Stainless Steel	Sigma Aldrich
Carbon Paper	Fuel Cell Store
Titanium Foil	Sigma Aldrich
Copper Foil	Sigma Aldrich

All electrochemical measurements were run in an Ar-filled glove box, with O_2 content less than 7 ppm and H_2O content less than 1 ppm.

1.2.2 ELECTROLYTES

Electrolyte solutions were made inside an Ar-filled glove box. Perchlorate salts were dissolved in 0 mM or 1 mM solutions of PMA in PC or CH_3CN (Table 4). Perchlorate salts are potential explosives, so precautions were taken to minimize dangers. Perchlorate salts were used as received and never dried or allowed to re-precipitate in solution.

Table 1.4: Perchlorate salts used in electrolytes with sources and concentrations.

Salt	Source	Concentrations (M)
$Mg(ClO_4)_2$	Alfa Aesar	0.1
		0.5
$LiClO_4$	Sigma Aldrich	0.5
$NaClO_4$	Alfa Aesar	0.5
$Ca(ClO_4)_2 \cdot 4H_2O$	Sigma Aldrich	0.5
$TBAClO_4$	Sigma Aldrich	0.1
		0.5

1.2.3 SURFACE EXPERIMENTS AND CELL DESIGN

Electrochemical measurements were performed using CH Instruments 760 D, 760 C, or 620 A Electrochemical Workstation (Austin, TX), and Biologic SP-150 (Claix, France). Cathode materials were studied using a three-electrode set up, where the cathode material was used as the working electrode, Mg foil (GalliumSource, LLC) was used as the reference electrode, and a polished glassy carbon electrode (CH Instruments) was used as the counter electrode. Glassy carbon electrodes were polished with 0.05 μm Al_2O_3 before use. Other counter electrodes were tested, including Mg foil and Au, Pt, and Ag wires. These counter electrodes were not chosen due to insufficient current due to passivation (Mg foil) or due to the introduction of unintended cations in solution. Cation impurities like Ag^+ or Au^{3+} could intercalate into the cathode materials and convolute findings. For these reasons, glassy carbon was chosen as the counter

electrode in half cell studies. Cells contained the cathode material clamped between an o-ring and Teflon-covered base. The cells were sealed with Parafilm during experiments and had an electrolyte volume of 2.5 mL and had less than 0.5 cm^3 of head space. Experiments were performed at 25 ºC, 35 °C, and 55 °C.

For solution studies, glassy carbon was used as the counter electrode, Mg foil was used as the reference electrode, and Pt wire was used as the working electrode. All Pt wires were cleaned in HNO_3 overnight to remove metal impurities and then heated in a hydrogen flame for 20 seconds before introduction into the glove box. The solution studies were performed in the glove box in a sealed glass vial with 4 mL of electrolyte and 0.5 cm^3 of head space.

For both cathode and solution studies, other reference electrodes were considered, including Li, Na, Ca (Gallium Source, LLC), Ag, and ferrocene. Li metal worked as a suitable reference and formed a non-passivating surface film, which conducted charge but was not reactive with the electrolytes. However, due to the high mobility of Li^+, possible contamination of Li^+ was possible in the electrolyte and in the cathode. Na metal is a strong base and is too reactive for use with CH_3CN electrolytes, forming H_2 gas upon contact. Ca metal is also reactive, and unlike Li, forms a passivating film which makes electrochemical half cell experiments difficult. Ag wire was considered as a quasi-reference electrode. However, the Ag quasi-reference drifted several hundred millivolts throughout an experiment, making peak potential assignments difficult. Ferrocene was considered as an internal standard, but the highly reversible redox couple Fc/Fc^+ occurs at potentials too positive relative to the electrochemical windows used in this study. Additionally, the ferrocene redox couple is known to be solvent dependent. One alternative would be to use decamethylferrocene which has a redox couple at -0.59 V

Fc/Fc^+. Although the internal standard is chemically inert, one must be careful that it would not overlap with the redox chemistry of interest.

For the reference and counter electrodes, fritted designs were considered to keep unwanted cations away from the cathode. These types of electrodes are commonly used in aqueous electrochemistry, such as the Ag/AgCl reference electrode. However, due to the cell size constraints and potential junction drop (due to differences in composition on either side of the frit), fritted designs were not used in final experiments.

1.2.4 SAMPLE CHARACTERIZATION

Scanning electron microscopy of the cathodes was performed using Hitachi S-4700 Cold FE-SEM (Hitachi High Technologies) with an acceleration voltage of 20 kV. Quantitative energy-dispersive X-ray spectroscopy (EDS) was performed with an Oxford Instruments ISIS EDS X-ray Microanalysis System using Cu foil as a standard. The cathodes were triple rinsed in CH_3CN after the experiment and dried in the glove box before analysis.

1.3 RESULTS AND DISCUSSION

1.3.1 AQUEOUS SOLUTION STUDIES

Figure 1.1 shows cyclic voltammograms of the solution waves of 5 mM PMA in an aqueous solution of 0.5 M $NaClO_4$. The redox peaks have been assigned previously to successive two-electron processes as shown in equations 1-3:[72,73,74]

$$[PMo_{12}O_{40}]^{3-} + 2e^- + 2H^+ \rightleftharpoons [H_2PMo_2{}^{V}Mo_{10}{}^{VI}O_{40}]^{3-} \quad (1)$$

$$[H_2PMo_2{}^{V}Mo_{10}{}^{VI}O_{40}]^{3-} + 2e^- + 2H^+ \rightleftharpoons [H_4PMo_4{}^{V}Mo_8{}^{VI}O_{40}]^{3-} \quad (2)$$

$$[H_6PMo_4{}^{V}Mo_8{}^{VI}O_{40}]^{3-} + 2e^- + 2H^+ \rightleftharpoons [H_6PMo_6{}^{V}Mo_6{}^{VI}O_{40}]^{3-} \quad (3)$$

Five redox features are visible in the cyclic voltammetry, and that this is likely due to anion effects. In 1 M H_3PO_4, four redox couples are observed,[74] and in H_2SO_4 three redox couples are seen.[72, 74] Additional features may be present in these other solution systems but were not visible due to the potential window chosen. The redox couples at E = -0.15 V vs. Ag/AgCl and E = -0.5 V vs. Ag/AgCl have entirely negative current and are not fully reversible.

The peak current (i_p) was investigated as a function of the square root of the scan rate. The first three redox peaks increase linearly with scan rate as expected (Figure 1.1B). This finding implies that the electrochemical process involves species in solution under diffusion-limited control.

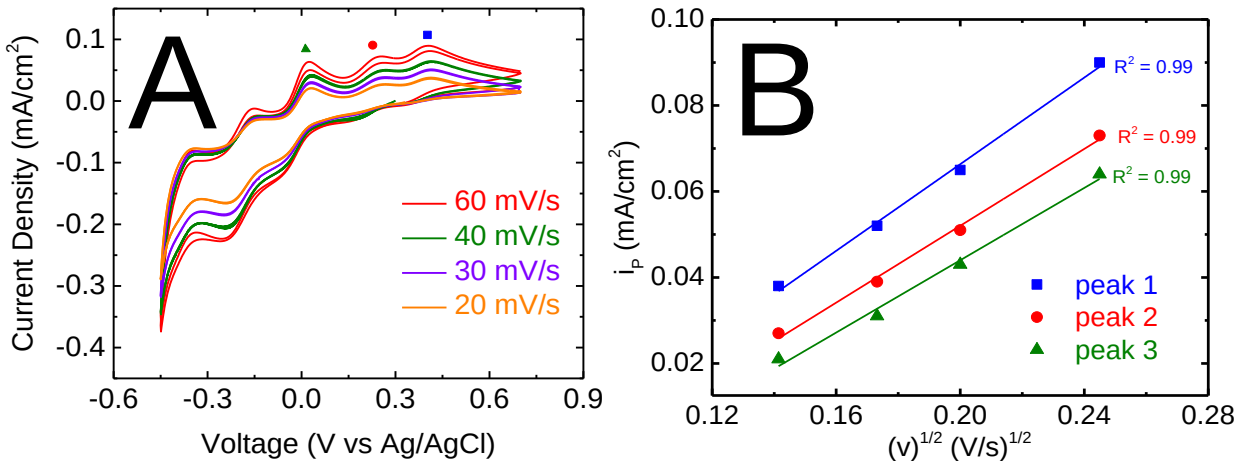


Figure 1.1: Cyclic voltammograms of 5 mM PMA in aqueous 0.5 M $NaClO_4$ at various scan rates: 60 mV/s (red), 50 mV/s (blue), 40 mV/s (green), 30 mV/s (purple), 20 mV/s (orange) (A). Randles-Sevcik plot of peak current plotted against the square root of the scan rate, where the first oxidative peak 1 (blue square), peak 2 (red circle), and peak 3 (green triangle) show a linear relationship (B). Linear fits are provided as a guide for the eye.

1.3.2 NONAQUEOUS SOLUTION STUDIES

We hypothesize that the PMA system's redox reactions will perform similarly in nonaqueous environments, following the general two-electron process:

$$[PMo_{12}{}^{VI}O_{40}]^{3-} + ne^- + nX^+ \rightleftharpoons [X_nPMo_n{}^{V}Mo_{12-n}{}^{VI}O_{40}]^{3-} \quad (4)$$

where n is equal to a multiple of two and X is an associating cation. We predict that TBA^+, Li^+, Na^+, Mg^{2+}, and Ca^{2+} will all associate with PMA, allowing the reversible reduction of PMA in solution and when bound to a surface.

To investigate the effect of non-aqueous solvents on the redox couples of PMA, the same study was repeated in PC. Figure 1.2A shows the cyclic voltammograms of PMA in PC at various scan rates. The initial peak at 1.6 V vs. Mg/Mg^{2+} is much larger than in aqueous studies. In the large electrochemical window, six reversible redox couples are identified at 1.76, 1.64, 1.46, 1.20, 0.86, and 0.53 V vs. Mg/Mg^{2+}.

There is no shift in peak potential with scan rate (Figure 1.2A). Figure 1.2B shows cyclic voltammograms of PMA in PC and CH_3CN. The peak potentials do not shift with solvent, but CH_3CN shows more reductive current overall.

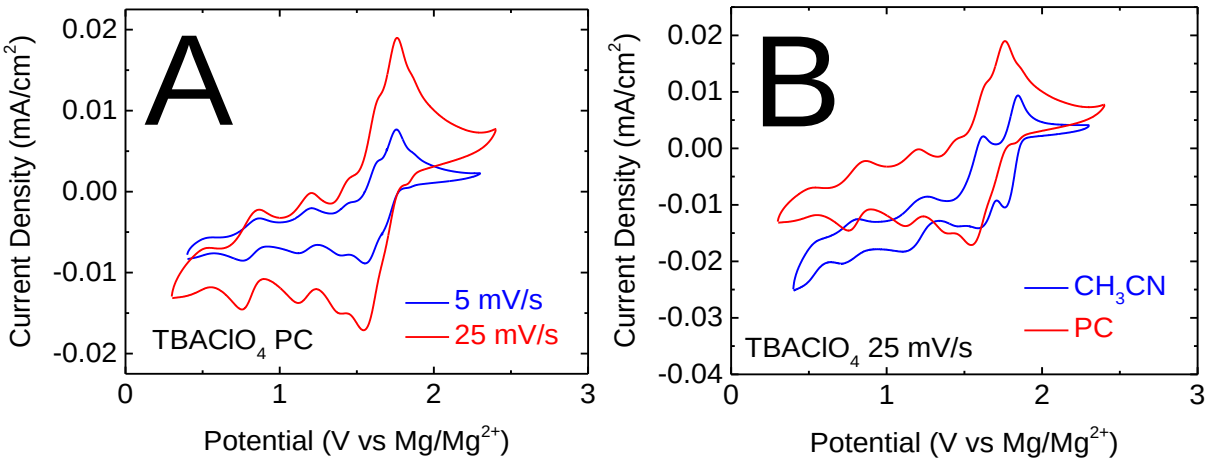


Figure 1.2: Cyclic Voltammograms of 1 mM PMA in 0.5 M $TBAClO_4$ in PC at 25 mV/s (A, red) and 5 mV/s (A, blue). Cyclic voltammograms of 1 mM PMA in CH_3CN (B, blue) and PC (B, red) at 25 mV/s.

1.3.3 CATION SOLUTION STUDIES IN PC

To determine if PMA could be used as a suitable cathode material in various battery systems, the effect of metal cation was tested in PC. Figure 1.3 shows cyclic voltammograms of PMA in PC, where the redox couples are due to the association with Li^+ and Mg^{2+} as described in equation 5 and 6:

$$[PMo_{12}{}^{VI}O_{40}]^{3-} + 2e^- + 2Li^+ \rightleftharpoons [Li_2PMo_2{}^{V}Mo_{10}{}^{VI}O_{40}]^{3-} \quad (5)$$

$$[PMo_{12}{}^{VI}O_{40}]^{3-} + 2e^- + Mg^{2+} \rightleftharpoons [MgPMo_2{}^{V}Mo_{10}{}^{VI}O_{40}]^{3-} \quad (6)$$

The current densities are similar, but the first oxidative wave in the Mg system is shifted 160 mV more negative than the Li system. This result suggests that PMA's association with Mg^{2+} is more facile than with Li^+, which is surprising due to the smaller charge of Li^+. The Li

system shows large reductive and oxidative current around 0.6 V vs. Mg/Mg^{2+}, which is not present in the Mg system. This feature is not attributed to Li deposition due to the high potential. Molybdenum salts have been used to reduce perchlorate to chloride, but this chemistry has been reported at significantly higher potentials.[75] We hypothesize that the large oxidative and reductive features in the Li electrochemistry may be influencing the PMA waves.

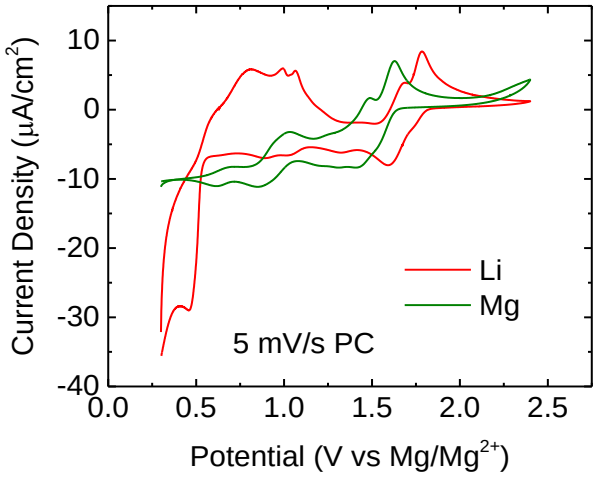


Figure 1.3: Cyclic Voltammograms of 1 mM PMA in PC with supporting electrolytes of 0.5 M $LiClO_4$ (red) and 0.5 M $Mg(ClO_4)_2$ (green) in PC with scan rates of 5 mV/s on a Pt working electrode, glassy carbon counter, and Mg foil reference.

When the electrochemical window of the Li system is limited to 0.7 V vs. Mg/Mg^{2+}, the first redox wave is shifted by 100 mV as opposed to 160 mV (Figure 1.4). It is possible that instead of observing a shift, a different redox series is observed. Perhaps, at 1.6 V vs. Mg/Mg^{2+} we observe the first redox wave of the Mg system and the second redox wave of the Li system (Figure 1.4 yellow). Because the redox wave at 1 V vs. Mg/Mg^{2+} (Figure 1.4 cyan) is the same for both the Li and Mg system, this finding suggests that the peaks are not shifted the same amount.

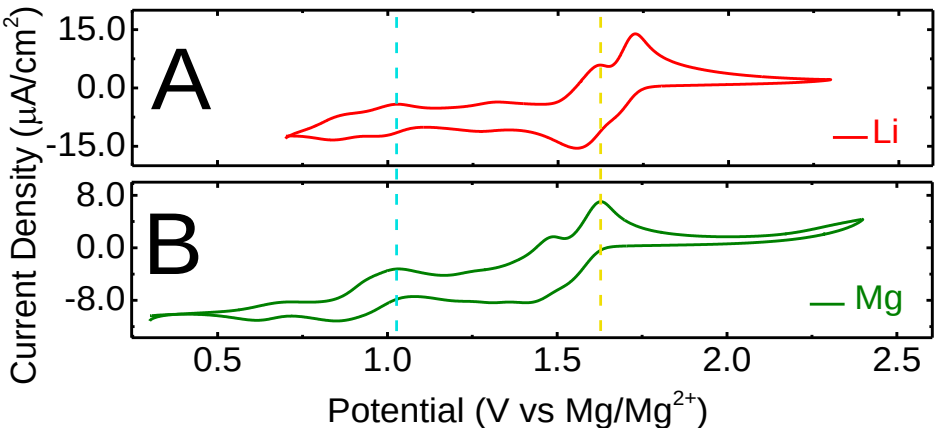


Figure 1.4: Cyclic voltammograms of 1 mM PMA in PC at a scan rate 5 mV/s in supporting electrolytes of 0.5 M $LiClO_4$ (red) and 0.5 M $Mg(ClO_4)_2$ (green). The cyan and yellow dashed lines are given as a guide to the eye at 1 and 1.6 V vs. Mg/Mg^{2+} respectively.

1.3.4 CATION SOLUTION STUDIES IN CH_3CN

The solution chemistry of PMA with different supporting salts was also studied in CH_3CN. The electrochemical behavior is significantly different compared to aqueous and PC electrolytes. Figure 1.5 illustrates this difference, showing cyclic voltammograms of PMA with $LiClO_4$, $Mg(ClO_4)_2$, and $NaClO_4$ supporting salts. A Na system was added as a comparison for singly charged species with larger radii. In both the Li and Mg systems, the overall current is predominately reductive, causing the yellow solutions to turn deep blue during the solution study. Reduced PMA is well-characterized by this deep blue color and has been widely used as an analytical tool.[76] We note here, that the voltammetry is not reversible. Similar to the PC system, at lower voltages Li shows large oxidative and reductive features that are not associated with PMA. Because these features occur in both PC and CH_3CN, they are not a solvent effect. The electrochemical behavior of PMA in 0.5 M $NaClO_4$ in CH_3CN shows decomposition at extreme potentials, suggesting that a smaller window is necessary to interrogate the association of Na.

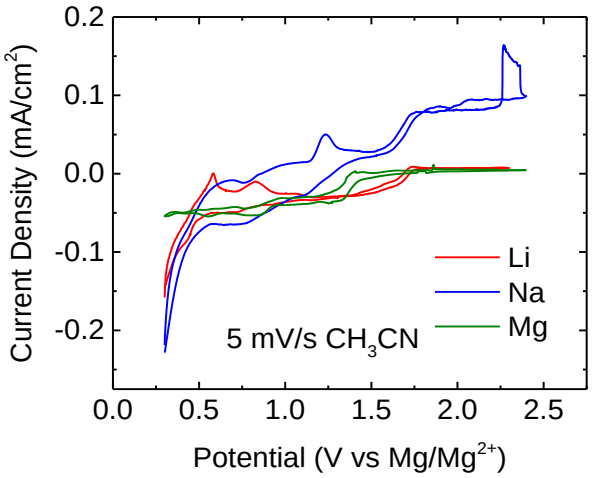


Figure 1.5: Cyclic voltammograms of 1 mM PMA in CH_3CN with various supporting electrolytes 0.5 M $LiClO_4$ (red), 0.5 M $NaClO_4$ (blue) and 0.5 M $Mg(ClO_4)_2$ (green) at a scan rate of 5 mV/s with Pt wire working, glassy carbon counter, and Mg foil reference.

When the range of voltages scanned is narrowed, the features associated with PMA are more defined in the solution studies in CH_3CN (Figure 1.6). All voltammograms show four redox waves, but the potential and reversibility vary.

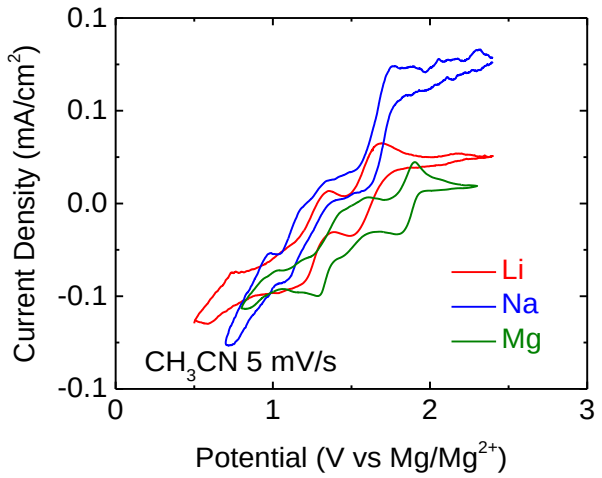


Figure 1.6: Cyclic voltammograms of 1 mM PMA in CH_3CN with various supporting electrolytes 0.5 M $LiClO_4$ (red), 0.5 M $NaClO_4$ (blue) and 0.5 M $Mg(ClO_4)_2$ (green) at a scan rate of 5 mV/s with Pt wire working, glassy carbon counter, and Mg foil reference.

1.3.5 POLYMER BINDER STUDIES

For a successful cathode material to intercalate different ions, the conductivity of the active material and binders must be considered. PMA is soluble in most solvents, and the process of confining polyoxometalates to surfaces has been well studied.

Figure 1.7 illustrates these differences in polymer conductivity. Cyclic voltammograms of PMA cathode materials with different polymer binders are shown. We note that PEO and PTFE show several reversible PMA redox features and high current densities relative to PVDF, PVP, and PANI. Because the electrolyte and active material (PMA) are the same, we believe these differences arise from polymer conductivity. If the polymer does not conduct Mg^{2+} ions well, the kinetics will be sluggish, which may be the case for the polymer PVDF. Future studies will use AC impedance to determine the conductivities of these binders.

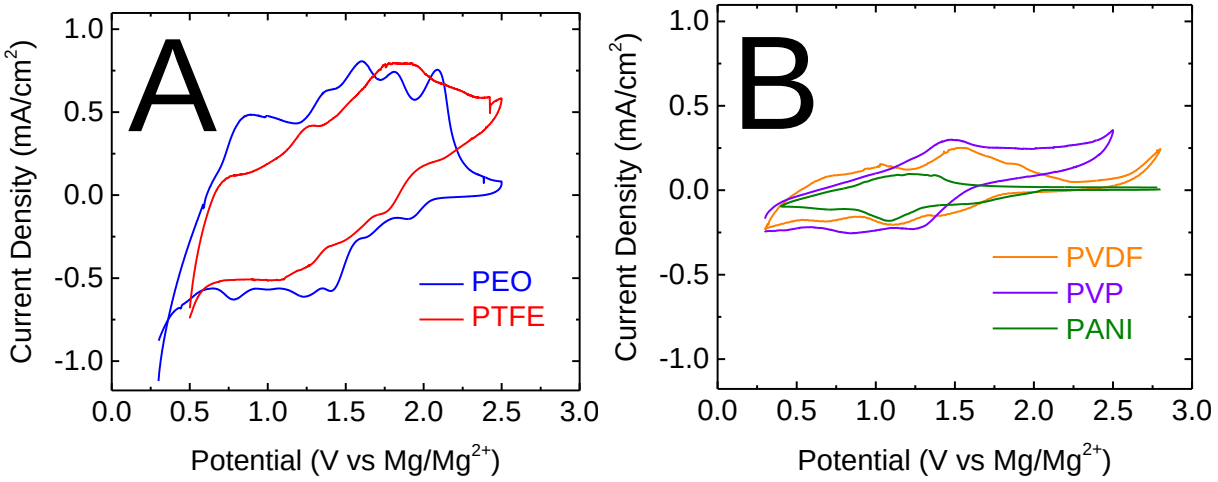


Figure 1.7: Cyclic voltammograms of PMA cathodes with poly ethylene oxide (blue, A), polytetrafluoroethylene (red, A), polyvinylidene fluoride (orange, B), polyvinylpyrrolidone (purple, B), and polyaniline (green, B). The scan rate was 5 mV/s, and the electrolyte was 0.1 M $TBAClO_4$ with 0.1 M $Mg(ClO_4)_2$ in CH_3CN.

1.3.6 TEMPERATURE STUDIES

Due to the kinetic barriers of reversibly intercalating small, charged species like Mg^{2+}, studies have shown that elevating the temperature improves reversibility and performance. Chevrel phase Mo_6S_8, the predominant cathode currently used in Mg-ion battery prototypes, is frequently studied at 55°C.[27] However, due to the moderate boiling points of CH_3CN (82°C) and THF (66°C), lower temperatures were chosen to avoid evaporating the solvent. As shown in Figure 1.8, the increase in temperature drastically changed the electrochemistry. At 35°C (Figure 1.8 red), the peaks are well-defined. At 25°C (Figure 1.8 blue), the electrochemistry is very resistive and poorly resolved.

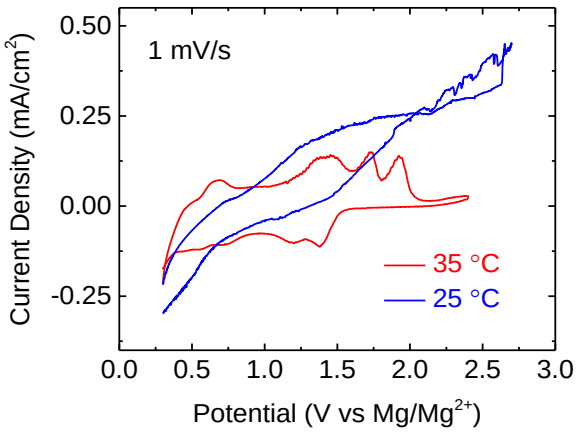


Figure 1.8: Cyclic voltammograms of 1:1:1 PMA:PEO:C cathode as the working electrode in 0.1 M $TBAClO_4$ with 0.1 M $Mg(ClO_4)_2$ in CH_3CN at various temperatures, 35°C (red), and 25°C (blue). Mg foil was used as the reference and glassy carbon was the counter electrode.

1.3.7 CARBON AND BINDER EFFECTS

Previous studies have shown that the carbon active material content is significant and that buckeyballs have been successful shown as a possible cathode material.[77] It is therefore important to show that activity in these systems is due to the PMA and not solely due to the

carbon support. Cathodes were cast in a similar method as described previously, however no active PMA was included in the slurry, and instead an equal weight of carbon was added. The cathode without PMA shows no electrochemical redox activity (Figure 1.9). This finding suggests that the PMA is responsible for the reversible redox waves.

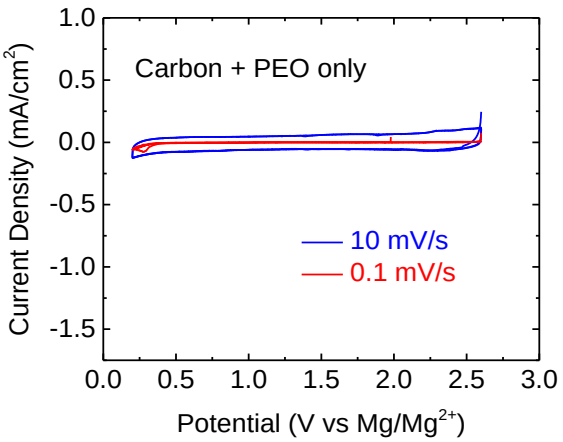


Figure 1.9: Cyclic voltammograms of 2:1 Carbon:PEO at various scan rates, 10 mV/s (blue) and 0.1 mV/s (red).

1.4 CONCLUSIONS

PMA was studied as a possible cathode material for Mg-ion batteries. Reversible solution waves of PMA in PC and CH_3CN suggest that PMA could associate with various cationic species at high voltages vs. Mg/Mg^{2+}. These studies suggest that reversible behavior occurs in a limited voltage window, and the reactivity beyond this is not well understood. PMA solubility was addressed by confining the polyoxometalate to the electrode surface using polymer binders. PEO was found to give the highest performing cathodes. Due to the sluggish kinetics of Mg^{2+} intercalation, increased temperature was found to be favorable.

1.5 REFERENCES

1. US Department of Energy, Energy Information Administration. Database, International Energy Statistics Database, Ed. 2014.

2. Blasing, T. Recent greenhouse gas concentrations. Carbon Dioxide Information Analysis Center, US Department of Energy, Ed. 2015.

3. Barthelmie, R.; Pryor, S. Potential contribution of wind energy to climate change mitigation. *Nature Clim. Change,* **2014,** *4*, 684-688.

4. Dunn, B.; Kamath, H.; Tarascon, J. Electrical Energy Storage for the Grid: A Battery of Choices. *Science,* **2011,** *334*, 928-935.

5. Tran, M.; Banister, D.; Bishop, J.; McCulloch, M. Realizing the electric-vehicle revolution. *Nature Clim. Change,* **2012,** *2*, 328-333.

6. Service, R. Bringing Fuel Cells Down to Earth. *Science*, **1999,** *285*, 682-685.

7. Lefèvre, M.; Proietti, E.; Jaouen, F.; Dodelet, J. Iron-Based Catalysts with Improved Oxygen Reduction Activity in Polymer Electrolyte Fuel Cells. *Science,* **2009,** *324*, 71-74.

8. Wu, G.; More, K.; Johnston, C.; Zelenay, P. High-Performance Electrocatalysts for Oxygen Reduction Derived from Polyaniline, Iron, and Cobalt. *Science,* **2011,** *332*, 443-447.

9. Nykvist, B.; Nilsson, M. Rapidly falling costs of battery packs for electric vehicles. *Nature Clim. Change,* **2015,** *5*, 329-332.

10. Wu, H.; Zhuo, D.; Kong, D.; Cui, Y. Improving battery safety by early detection of internal shorting with a bifunctional separator. *Nat. Commun.,* **2014,** *5*, 1-6.

11. Yoo, H.; Shterenberg, I.; Gofer, Y.; Gershinsky, G.; Pour, N.; Aurbach, D. Mg rechargeable batteries: an on-going challenge. *Energy Environ. Sci.,* **2013,** *6*, 2265-2279.

12. Gregory, T.; Hoffman, R.; Winterton, R. Nonaqueous Electrochemistry of Magnesium: Applications to Energy Storage. *J. Electrochem. Soc.,* **1990,** *137*, 775-780.

13. Aurbach, D.; Lu, Z.; Schechter, A.; Gofer, Y.; Gizbar, H.; Turgeman, R.; Cohen, Y.; Moshkovich, M.; Levi, E. Prototype systems for rechargeable magnesium batteries. *Nature*, **2000,** *407*, 724-727.

14. Shterenberg, I.; Salama, M.; Gofer, Y.; Levi, E.; Aurbach, D. The challenge of developing rechargeable magnesium batteries. *MRS Bull.,* **2014,** *39*, 453-460.

15. Saha, P.; Datta, M.; Velikokhatnyi, O.; Manivannan, A.; Alman, D.; Kumta, P. Rechargeable magnesium battery: Current status and key challenges for the future. *Prog. Mater Sci.,* **2014,** *66*, 1-86.

16. Barile, C.; Spatney, R.; Zavadil, K.; Gewirth, A. Investigating the Reversibility of in Situ Generated Magnesium Organohaloaluminates for Magnesium Deposition and Dissolution. *J. Phys. Chem. C,* **2014,** *118*, 10694-10699.

17. Muldoon, J.; Bucur, C.; Gregory, T. Quest for Nonaqueous Multivalent Secondary Batteries: Magnesium and Beyond. *Chem. Rev.*, **2014,** *114*, 11683-11720.

18. Mizrahi, O.; Amir, N.; Pollak, E.; Chusid, O.; Marks, V.; Gottlieb, H.; Larush, L.; Zinigrad, E.; Aurbach, D. Electrolyte Solutions with a Wide Electrochemical Window for Rechargeable Magnesium Batteries. *J. Electrochem. Soc.*, **2008,** *155*, A103-A109.

19. Benmayza, A.; Ramanathan, M.; Arthur, T.; Matsui, M.; Mizuno, F.; Guo, J.; Glans, P.; Prakash, J. Effect of Electrolytic Properties of a Magnesium Organohaloaluminate Electrolyte on Magnesium Deposition. *J. Phys. Chem. C,* **2013,** *117*, 26881-26888.

20. Liu, T.; Shao, Y.; Li, G.; Gu, M.; Hu, J.; Xu, S.; Nie, Z.; Chen, X.; Wang, C.; Liu, J. A facile approach using $MgCl_2$ to formulate high performance Mg^{2+} electrolytes for rechargeable Mg batteries. *J. Mater. Chem. A,* **2014,** *2*, 3430-3438.

21. Doe, R.; Han, R.; Hwang, J.; Gmitter, A.; Shterenberg, I.; Yoo, H.; Pour, N.; Aurbach, D. Novel electrolyte solutions comprising fully inorganic salts with high anodic stability for rechargeable magnesium batteries. *Chem. Commun.,* **2014,** *50*, 243-245.

22. Barile, C.; Barile, E.; Zavadil, K.; Nuzzo, R.; Gewirth, A. Electrolytic Conditioning of a Magnesium Aluminum Chloride Complex for Reversible Magnesium Deposition. *J. Phys. Chem. C,* **2014,** *118*, 27623-27630.

23. Zhang, R.; Yu, X.; Nam, K.; Ling, C.; Arthur, T.; Song, W.; Knapp, A.; Ehrlich, S.; Yang, X.; Matsui, M. α-MnO2 as a cathode material for rechargeable Mg batteries. *Electrochem. Commun.*, **2012,** *23*, 110-113.

24. Novák, P.; Scheifele, W.; Joho, F.; Haas, O. Electrochemical Insertion of Magnesium into Hydrated Vanadium Bronzes. *J. Electrochem. Soc.*, **1995,** *142*, 2544-2550.

25. Ichitsubo, T.; Yagi, S.; Nakamura, R.; Ichikawa, Y.; Okamoto, S.; Sugimura, K.; Kawaguchi, T.; Kitada, A.; Oishi, M.; Doi, T.; Matsubara, E., A new aspect of Chevrel compounds as positive electrodes for magnesium batteries. *J. Mater. Chem. A,* **2014,** *2*, 14858-14866.

26. Choi, S.; Kim, J.; Woo, S.; Cho, W.; Choi, S. Y.; Choi, J.; Lee, K.; Park, M.; Kim, Y. Role of Cu in Mo_6S_8 and Cu Mixture Cathodes for Magnesium Ion Batteries. *Acs. Appl. Mater. Inter.*, **2015,** *7*, 7016-7024.

27. Levi, E.; Gofer, Y.; Vestfreed, Y.; Lancry, E.; Aurbach, D. $Cu_2Mo_6S_8$ Chevrel Phase, A Promising Cathode Material for New Rechargeable Mg Batteries: A Mechanically Induced Chemical Reaction. *Chem. Mater.*, **2002,** *14*, 2767-2773.

28. Babu, G.; Ababtain, K.; Ng, K.; Arava, L. Electrocatalysis of Lithium Polysulfides: Current Collectors as Electrodes in Li/S Battery Configuration. *Sci. Rep.*, **2015,** *5*, 1-7.

29. Nakamura, H.; Ogawa, Y.; Gunji, K.; Kasahara, A. Ionic and Positive Hole Conductivities of Solid Magnesium and Strontium Sulfides. *T. Jpn I. Met.,* **1984,** *25*, 692-697.

30. Higashi, S.; Miwa, K.; Aoki, M.; Takechi, K. A novel inorganic solid state ion conductor for rechargeable Mg batteries. *Chem. Commun.,* **2014,** *50*, 1320-1322.

31. Banks, E.; Russo, V.; Ward, R. The Preparation of Pure Magnesium Sulfide and its Use as a Base Material for Infrared Phosphors. *J.A.C.S.,* **1950,** *72*, 3173-3176.

32. Xu, Y.; Xiao, X. Accelerated microwave synthesis of magnesium sulfide with the pro-heating medium of graphite. *J. Mater. Res.,* **1995,** *10*, 334-338.

33. Kim, H.; Arthur, T.; Allred, G.; Zajicek, J.; Newman, J.; Rodnyansky, A.; Oliver, A.; Boggess, W.; Muldoon, J. Structure and compatibility of a magnesium electrolyte with a sulphur cathode. *Nat. Commun.,* **2011,** *2*, 427.

34. Novák, P.; Imhof, R.; Haas, O. Magnesium insertion electrodes for rechargeable nonaqueous batteries — a competitive alternative to lithium? *Electrochim. Acta.,* **1999,** *45*, 351-367.

35. Jiao, L.; Yuan, H.; Si, Y.; Wang, Y.; Cao, J.; Gao, X.; Zhao, M.; Zhou, X.; Wang, Y. Electrochemical insertion of magnesium in open-ended vanadium oxide nanotubes. *J. Power Sources,* **2006,** *156*, 673-676.

36. Imamura, D.; Miyayama, M. Characterization of magnesium-intercalated V_2O_5/carbon composites. *Solid State Ionics,* **2003,** *161*, 173-180.

37. Song, J.; Noked, M.; Gillette, E.; Duay, J.; Rubloff, G.; Lee, S. Activation of a MnO_2 cathode by water-stimulated Mg^{2+} insertion for a magnesium ion battery. *Phys. Chem. Chem. Phys.,* **2015,** *17*, 5256-5264.

38. Rasul, S.; Suzuki, S.; Yamaguchi, S.; Miyayama, M. High capacity positive electrodes for secondary Mg-ion batteries. *Electrochim. Acta.,* **2012,** *82*, 243-249.

39. Rasul, S.; Suzuki, S.; Yamaguchi, S.; Miyayama, M. Synthesis and electrochemical behavior of hollandite MnO_2/acetylene black composite cathode for secondary Mg-ion batteries. *Solid State Ionics,* **2012,** *225*, 542-546.

40. Orikasa, Y.; Masese, T.; Koyama, Y.; Mori, T.; Hattori, M.; Yamamoto, K.; Okado, T.; Huang, Z.; Minato, T.; Tassel, C.; Kim, J.; Kobayashi, Y.; Abe, T.; Kageyama, H.; Uchimoto, Y. High energy density rechargeable magnesium battery using earth-abundant and non-toxic elements. *Sci. Rep.,* **2014,** *4*, 1-6.

41. Pope, M. T.; Müller, A. Polyoxometalate Chemistry: An Old Field with New Dimensions in Several Disciplines. *Angew. Chem. Int. Ed.,* **1991,** *30*, 34-48.

42. Hill, C. Introduction: PolyoxometalatesMulticomponent Molecular Vehicles To Probe Fundamental Issues and Practical Problems. *Chem. Rev.,* **1998,** *98*, 1-2.

43. Long, D.; Tsunashima, R.; Cronin, L. Polyoxometalates: Building Blocks for Functional Nanoscale Systems. *Angew. Chem. Int. Ed.,* **2010,** *49*, 1736-1758.

44. Maayan, G.; Popovitz-Biro, R.; Neumann, R. Micelle Directed Synthesis of Polyoxometalate Nanoparticles and Their Improved Catalytic Activity for the Aerobic Oxidation of Sulfides. *J.A.C.S.,* **2006,** *128*, 4968-4969.

45. Li, S.; Wang, E.; Tian, C.; Mao, B.; Song, Y.; Wang, C.; Xu, L. In situ fabrication of amino acid-polyoxometalate nanoparticle functionalized ultrathin films and relevant electrochemical property study. *Mater. Res. Bull.,* **2008,** *43*, 2880-2886.

46. Wang, S.; Liu, L.; Chen, W.; Zhang, Z.; Su, Z.; Wang, E. A new electrodeposition approach for preparing polyoxometalates-based electrochromic smart windows. *J. Mater. Chem. A,* **2013,** *1*, 216-220.

47. Genovese, M.; Lian, K. Polyoxometalate modified inorganic–organic nanocomposite materials for energy storage applications: A review. *Curr. Opin. Solid State Mater. Sci.,* **2015,** *19*, 126-137.

48. Busche, C.; Vila-Nadal, L.; Yan, J.; Miras, H.; Long, D.; Georgiev, V.; Asenov, A.; Pedersen, R.; Gadegaard, N.; Mirza, M.; Paul, D.; Poblet, J.; Cronin, L. Design and fabrication of memory devices based on nanoscale polyoxometalate clusters. *Nature,* **2014,** *515*, 545-549.

49. Liu, D.; Lu, Y.; Tan, H.; Chen, W.; Zhang, Z.; Li, Y.; Wang, E. Polyoxometalate-based purely inorganic porous frameworks with selective adsorption and oxidative catalysis functionalities. *Chem. Commun.,* **2013,** *49*, 3673-3675.

50. Kozhevnikov, I. Catalysis by Heteropoly Acids and Multicomponent Polyoxometalates in Liquid-Phase Reactions. *Chem. Rev.,* **1998,** *98*, 171-198.

51. Geisberger, G.; Paulus, S.; Carraro, M.; Bonchio, M.; Patzke, G. Synthesis, Characterisation and Cytotoxicity of Polyoxometalate/Carboxymethyl Chitosan Nanocomposites. *Chem. Eur. J.,* **2011,** *17*, 4619-4625.

52. Lira-Cantú, M.; Gómez-Romero, P. Electrochemical and Chemical Syntheses of the Hybrid Organic−Inorganic Electroactive Material Formed by Phosphomolybdate and Polyaniline. Application as Cation-Insertion Electrodes. *Chem. Mater.,* **1998,** *10*, 698-704.

53. Wang, H.; Hamanaka, S.; Nishimoto, Y.; Irle, S.; Yokoyama, T.; Yoshikawa, H.; Awaga, K. In Operando X-ray Absorption Fine Structure Studies of Polyoxometalate Molecular Cluster Batteries: Polyoxometalates as Electron Sponges. *J.A.C.S.,* **2012,** *134*, 4918-4924.

54. Genovese, M.; Foong, Y.; Lian, K. Designing Polyoxometalate based Layer-by-Layer Thin Films on Carbon Nanomaterials for Pseudocapacitive Electrodes. *J. Electrochem. Soc.,* **2015,** *162*, A5041-A5046.

55. Siné, G.; Hui, C.; Kuhn, A.; Kulesza, P.; Miecznikowski, K.; Chojak, M.; Paderewska, A.; Lewera, A. Spatial Control of Polyaniline Electrodeposition by Patterned Polyoxometalate Monolayers. *J. Electrochem. Soc.,* **2003,** *150*, C351-C355.

56. Choi, K.; Choi, S.; Kim, J. Electrocatalysis of Oxygen Reduction by Au Nanoparticles Electrodeposited on Polyoxometalate-Modified Electrode Surfaces. *J. Korean Electrochem. Soc.*, **2009,** *12*, 75-80.

57. Abdel-Samiea, B.; Gamal, R.; Sheha, E. All-solid-state polymer electrolyte with plastic crystal materials for rechargeable magnesium battery. *Cleantech*, **2012**, *1*, 164-169.

58. Sharma, J.; Hashmi, S. Magnesium ion transport in poly(ethylene oxide)-based polymer electrolyte containing plastic-crystalline succinonitrile. *J. Solid State Electrochem.,* **2013,** *17*, 2283-2291.

59. Agrawal, R.; Sahu, D. Mg^{2+}-ion Conducting Polymer Electrolytse: Materials Characterization and All-Solid-State Battery Performance Studies. *J. Phys. Chem. App.,* **2013,** *3*, 9-17.

60. Perween, M.; Gupta, R.; Rebary, B.; Kulshrestha, V.; Srivastava, D. Effective management of passive layers using composite cathodes in solid state magnesium batteries. *Phys. Chem. Chem. Phys.,* **2013,** *15*, 17758-17762.

61. Chusid, O.; Gofer, Y.; Gizbar, H.; Vestfrid, Y.; Levi, E.; Aurbach, D.; Riech, I. Solid-State Rechargeable Magnesium Batteries. *Adv. Mater.,* **2003,** *15*, 627-630.

62. Huggins, R. A. Simple method to determine electronic and ionic components of the conductivity in mixed conductors a review. *Ionics,* **2002,** *8*, 300-313.

63. Qian, X.; Gu, N.; Cheng, Z.; Yang, X.; Wang, E.; Dong, S. Methods to study the ionic conductivity of polymeric electrolytes using a.c. impedance spectroscopy. *J. Solid State Electrochem.,* **2001,** *6*, 8-15.

64. Günter, J.; Bensch, W. Two new trigonal magnesium heteropolytungstates: Crystal structures, topotactic relations, and thermal dehydration. *J. Solid State Chem.,* **1987,** *69*, 202-214.

65. Günter, J.; Schmalle, H.; Dubler, E. Crystal structure and properties of a new magnesium heteropoly-tungstate, $Mg_7(MgW_{12}O_{42})(OH)_4(H_2O)_8$, and the isostructural compounds of manganese, iron, cobalt and nickel. *Solid State Ionics,* **1990,** *43*, 85-92.

66. Tatibouët, J. M.; Montalescot, C.; Brückman, K.; Haber, J.; Che, M. A Two-Step Transformation of the Magnesium Salt of Phosphomolybdic Acid $HMgPMo_{12}O_{40}$ Supported on Silica. *J. Catal.,* **1997,** *169*, 22-32.

67. Pratt, H.; Hudak, N.; Fang, X.; Anderson, T. A polyoxometalate flow battery. *J. Power Sources,* **2013,** *236*, 259-264.

68. Ni, E.; Uematsu, S.; Sonoyama, N. Anderson type polyoxomolybdate as cathode material of lithium battery and its reaction mechanism. *J. Power Sources*, **2014,** *267*, 673-681.

69. Wang, H.; Yamada, T.; Hamanaka, S.; Yoshikawa, H.; Awaga, K. Cathode Composition Dependence of Battery Performance of Polyoxometalate (POM) Molecular Cluster Batteries. *Chem. Lett.*, **2014,** *43*, 1067-1069.

70. Yang, H.; Song, T.; Liu, L.; Devadoss, A.; Xia, F.; Han, H.; Park, H.; Sigmund, W.; Kwon, K.; Paik, U. Polyaniline/Polyoxometalate Hybrid Nanofibers as Cathode for Lithium Ion Batteries with Improved Lithium Storage Capacity. *J. Phys. Chem. C*, **2013,** *117*, 17376-17381.

71. Kawasaki, N.; Wang, H.; Nakanishi, R.; Hamanaka, S.; Kitaura, R.; Shinohara, H.; Yokoyama, T.; Yoshikawa, H.; Awaga, K. Nanohybridization of Polyoxometalate Clusters and Single-Wall Carbon Nanotubes: Applications in Molecular Cluster Batteries. *Angew. Chem. Int. Ed.*, **2011,** *50*, 3471-3474.

72. Lewera, A.; Chojak, M.; Miecznikowski, K.; Kulesza, P. Identification and Electroanalytical Characterization of Redox Transitions in Solid-State Keggin type Phosphomolybdic Acid. *Electroanal.*, **2005,** *17*, 1471-1476.

73. Guo, H.; Li, Y.; Fan, L.; Wu, X.; Guo, M., Voltammetric behavior study of folic acid at phosphomolybdic-polypyrrole film modified electrode. *Electrochim. Acta.*, **2006,** *51*, 6230-6237.

74. Symes, M.; Cronin, L. Decoupling hydrogen and oxygen evolution during electrolytic water splitting using an electron-coupled-proton buffer. *Nat. Chem.*, **2013,** *5*, 403-409.

75. Rechnitz, G.; Laitinen, H. A Study of the Molybdenum Catalyzed Reduction of Perchlorate. *Anal. Chem.*, **1961,** *33*, 1473-1477.

76. Boltz, D.; Mellon, M. Determination of Phosphorus, Germanium, Silicon, and Arsenic. *Anal. Chem.*, **1947,** *19*, 873-877.

77. Zhang, R.; Mizuno, F.; Ling, C. Fullerenes: non-transition metal clusters as rechargeable magnesium battery cathodes. *Chem. Commun.*, **2015,** *51*, 1108-1111.

Chapter 2: Electrochemical Insight into Mg Deposition and Dissolution Pathways

Reprinted (adapted) with permission from (Barile, C.; Barile, E.; Zavadil, K.; Nuzzo, R.; Gewirth, A. Electrolytic Conditioning of a Magnesium Aluminum Chloride Complex for Reversible Magnesium Deposition. *J. Phys. Chem. C,* **2014,** *118*, 27623-27630.). Copyright (2014) American Chemical Society.

2.1 INTRODUCTION

Mg-ion batteries have attracted much attention in the past decade due to their high theoretical volumetric capacity (3833 mAh/cm^3) compared to current Li-ion batteries using graphite anodes (850 mAh/cm^3).[1,2] One of the largest challenges in the commercialization of Mg-ion batteries is the development of a suitable electrolyte that is compatible with a Mg anode.[3] An ideal electrolyte would have a large electrochemical window, low flammability and cost, high conductivity, and support reversible Mg deposition.[4] A useful Mg electrolyte would also have comparable stability to those found in Li-ion systems. In Li-ion batteries, the ratio of charge passed during stripping to that passed during deposition (the Coulombic efficiency) is well over 99%.[5,6]

Over the past twenty years, the performance and chemical stability of Mg-electrolyte systems have improved markedly. Simple Grignard reagents were the first reported class of electrolytes to support reversible Mg deposition.[7,8] Grignard-based electrolytes, however, suffer from poor anodic stability and high chemical reactivity. Seminal work by Aurbach and coworkers led to the development of Mg organohaloaluminate-based electrolytes.[9] By tuning the organic substituents of these electrolytes, electrochemical windows of ~2.5 V combined with good Coulombic efficiencies have been reported.[10] Recently, Aurbach et al. and Liu et al.

developed an inorganic-based electrolyte, from $MgCl_2$ and $AlCl_3$ in ether solvents (MACC), which supports reversible Mg deposition with an anodic stability >3.0 V.[11,12] This system is promising because it can be coupled to high voltage Mg cathodes, though these are as yet to be discovered.

Previous work has demonstrated the profound impact of electrochemical cycling on the performance of Mg electrolytes. For example, the Coulombic efficiency ranges from 55% to 100% for $Mg(AlCl_2EtBu)_2$ depending on cycle number.[13] Aurbach et al. recently revealed that the electrochemical behavior of the MACC electrolyte also varies with cycling.[14] However, this process is not well understood.

In this work, the electrochemical and compositional properties of MACC systems are carefully examined as it cycles through sequences of metal deposition and dissolution. Electrode surface and solution changes of the MACC are explored during cycling and under resting conditions. The data from these studies establish important features of the mechanisms that support reversible Mg deposition from the MACC system.

2.2 EXPERIMENTAL DETAILS

2.2.1 GENERAL PROCEDURES

All chemicals were purchased from Sigma-Aldrich unless otherwise stated. All glassware was dried in an oven for at least 2 hours at 175°C and then flamed dried with a Bunsen burner before introduction into a glove box. THF was distilled over Na and benzophenone under Ar and dried over molecular sieves (3 Å) before use. The water content of THF, measured using Karl-Fischer titration, was found to be (7 ± 1) ppm, similar to literature values.[15] Wet-THF was never tested in this system, and the effect of water has not been carefully investigated. PolyTHF had a number average molecular weight of 2900. All materials were handled in an Ar-filled glove box.

Pt or Pd wires with immersed geometric surface areas of ~0.6 cm^3 (Alfa-Aesar) were used as working electrodes unless otherwise specified. Pt wires were cleaned in concentrated HNO_3 for at least 24 hours before each experiment. The use of abrasives to polish the Pt wire would leave Mg and Si contamination imbedded in the wire. Fresh Pd wires were used for each experiment. Because effective cleaning procedures to clean Mg from the Pd surface could not be found or established, new wires were used for each experiment. Following acid cleaning, all working electrodes were rinsed with Milli-Q water (>18 MΩ cm^{-1}) and annealed with a H_2 flame for 30-60 s prior to introduction into the glove box. The freshly flamed Pt wires were not placed in Milli-Q water, as is the convention when cleaning Pt for aqueous studies. This step was omitted to minimize the amount of adsorbed H_2O on the Pt surface.

Mg foil (GalliumSource, LLC) was used as the counter and reference electrodes, and all potentials were measured with respect to Mg/Mg^{2+}. Mg foil forms a native oxide, and no efforts were made to remove or polish the Mg foil. The foil was used as received. Electrochemistry was performed using a CH Instruments 760 D, 600 D, 760 C, or 620 A Electrochemical Workstation

(Austin, TX). Electrochemical cells were assembled in the glove box, sealed prior to use, and contained ~1.5 mL of electrolyte and ~0.5 cm^3 of head space. Increased electrode surface area relative to the volume of electrolyte, drastically affected the electrochemical performance. All studies were performed in mass spectrometry vials. Other studies, not reported here, used larger volumes and cell designs of various materials including Teflon and quartz. We find that electrolyte is sensitive to these changes and may require different protocols to achieve fully reversible behavior.

Coulombic efficiencies were calculated by dividing the integrated anodic current up to 2.8 V by the integrated cathodic current.

2.2.2 SYNTHESIS OF MAGNESIUM ALUMINUM CHLORIDE COMPLEX (MACC)

Nominally anhydrous $MgCl_2$ (Alfa Aesar) was dried in a tube furnace under a flowing Ar and HCl atmosphere at ~1 L/min for 2.5 hours at 300°C. The tube furnace was cooled to room temperature, and the gas flow was replaced with Ar only. The tube was sealed and then transferred into the glove box. The dry HCl gas was made by adding concentrated HCl into concentrated H_2SO_4 dropwise, and the formed HCl gas was bubbled twice through concentrated H_2SO_4 before it entered the tube furnace. As received $MgCl_2$ was never tested during the development of the synthesis protocol.

Under an inert atmosphere, THF (50 mL) was added to $AlCl_3$ (400 mg) dropwise at ~0°C over the course of ~30 min, using a Peltier plate inside the glovebox. $AlCl_3$ reacts exothermically with THF, and the slow dropwise addition helps prevent oligomer formation. THF (50 mL) was added to $MgCl_2$ (570 mg), and the resulting suspension was stirred at room temperature for at least 30 min. The $AlCl_3$-THF solution was then added dropwise at room temperature to the

$MgCl_2$-THF suspension over the course of ~30 min. The reaction mixture was then stirred for at least 6 hours at room temperature to form the MACC with a nominal concentration of 30 mM.

Analogous procedures were followed for preparing MACC in 1,2-dimethoxyethane (DME) and in THF with different $MgCl_2$-$AlCl_3$ ratios. Elemental analyses by ICP-AES were performed by the microanalysis laboratory located at the University of Illinois at Urbana-Champaign.

2.2.3 MASS SPECTROMETRY EXPERIMENTS

For mass spectrometry (MS) experiments, the electrolytes were diluted with additional THF, removed from the glove box in a sealed vial, and directly injected into a Quattro Ultima (Waters) electrospray ionization (ESI) mass spectrometer using a purged, Ar-filled syringe. MS was performed in positive ionization mode. Control experiments with blank THF showed no peaks associated with oligomerization. For MS experiments with the MACC in DME, electrolytes were evaporated in the glove box and redissolved in THF prior to examination by MS. We found that the DME solvent peak obscured MS analysis.

2.2.4 SCANNING ELECTRON MICROSCOPY

Scanning electron microscopy (SEM) of the electrodes was performed using a Hitachi S-4700 Cold FE-SEM (Hitachi High Technologies) with an acceleration voltage of 20 kV. Quantitative energy-dispersive X-ray spectroscopy (EDS) was performed with an Oxford Instruments ISIS EDS X-ray Microanalysis System using Cu foil as a standard. The surfaces were rinsed thoroughly with THF inside the glove box before transferring them for SEM-EDS analysis.

2.3 RESULTS AND DISCUSSION

2.3.1 MACC CONDITIONING

Figure 2.1 shows cyclic voltammograms of reversible Mg electrodeposition and stripping from a fully conditioned solution (*vide infra*) containing 30 mM of the MACC in THF on a Pt working electrode. As previously reported, the overpotential for deposition in this electrolyte is ~200 mV, and the Coulombic efficiency is nearly 100%.[12] Of further note, the electrochemical window of this electrolyte is greater than 3.0 V.

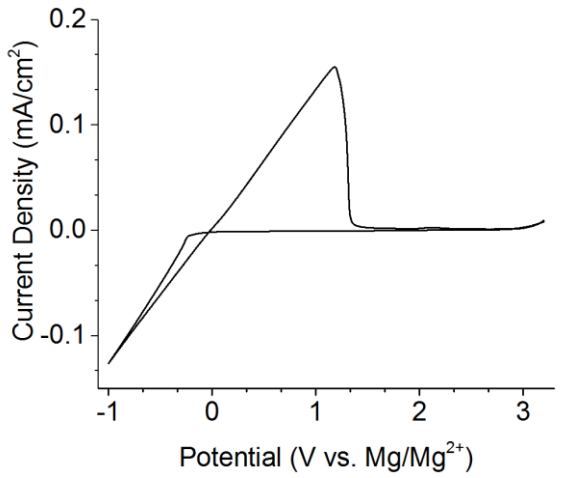


Figure 2.1: Cyclic voltammogram of the conditioned MACC in THF at 25 mV/s on a Pt electrode.

It is known that the freshly synthesized MACC cannot support reversible Mg electrodeposition and stripping (Figure 2.2A, black).[1] Aurbach et al. have shown that MACC electrolytes exhibiting high Coulombic efficiencies are attained after extensive electrochemical cycling, a process known as conditioning.[14] Figure 2.2A shows the changes in the electrochemical behavior of the MACC throughout a typical conditioning process. During the first cycles, reductive processes occur at an onset much greater than 0 V, and little oxidative current is measured (Figure 2.2A, black). This reductive current cannot be due to Mg deposition and is attributed to Al deposition on the working electrode and other irreversible processes.

Interestingly, an anodic feature is observed peaking at 2.2 V. With continued cycling, a reductive feature ascribed to Mg deposition and a corresponding stripping peak appear and evolve in character (Figure 2.2A, red). At the same time, additional anodic features at 2.5 V grow in before decreasing in intensity. We hypothesize that this feature is related to oligomer formation or of a species reversibly adsorbing to the surface. The feature traces over itself, which is not common for typical electrochemical behavior. Figure 2.2B shows that the onset of Mg deposition decreases to a constant value of ~200 mV during conditioning.

The Coulombic efficiency also improves during cycling (Figure 2.2B). During the first thirty cycles, Al and Mg codeposit causing the efficiency to increase from 0 to 70%. Since the Al deposition is only partially reversible, Al depletes from solution, resulting in a diminished Al stripping current. Perhaps the Al depletion causes the decrease in efficiency over the next forty cycles. Once the voltammetry is dominated by Mg deposition and stripping in the last eighty cycles, the Coulombic efficiency approaches 100%. Figure 2.2B shows that the MACC electrolyte exhibits high Coulombic efficiency once the deposition overpotential plateaus to ~200 mV.

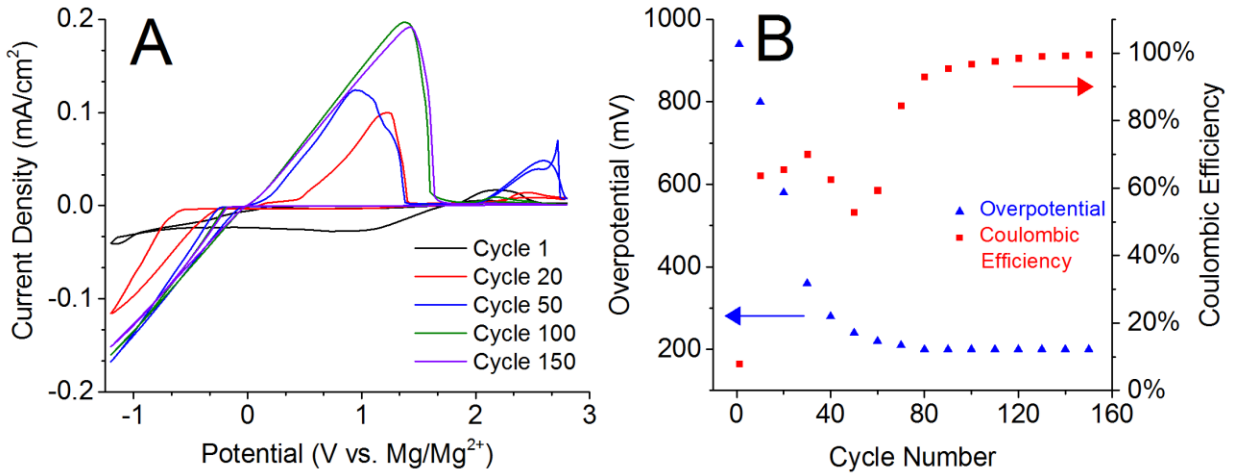


Figure 2.2: Cyclic voltammograms of cycle 1 (black), cycle 20 (red), cycle 50 (blue), cycle 100 (green), cycle 150 (purple) of the MACC in THF at 5 mV/s on a Pt electrode (A). Mg deposition overpotential and Coulombic efficiency as a function of cycle number (B).

To investigate the origin of the improvement in MACC performance with electrode cycling, a new Pt or Pd working electrode was introduced following MACC conditioning. If electrode surface conditioning is the origin of the increase in MACC performance, one would expect the working electrode to control the electrochemical behavior. Figure 2.3 shows cyclic voltammograms obtained following the introduction of fresh Pt or Pd surfaces into the conditioned MACC. Only minor differences distinguish the voltammograms of the new surfaces relative to the original Pt surface, particularly in the Mg deposition region. These differences may possibly be associated with impurities on the surface of the new electrodes and disappear with continued cycling. However, the Coulombic efficiency of the Mg deposition and stripping process ranges between 96-100% in all cases. This result suggests that the electrode surface does not participate in the electrolyte conditioning process directly. Correspondingly, we conclude that the solution composition changes during conditioning. We find that cells containing relatively small volumes of electrolyte and large working electrodes condition faster, which is consistent with a solution-dependent process.

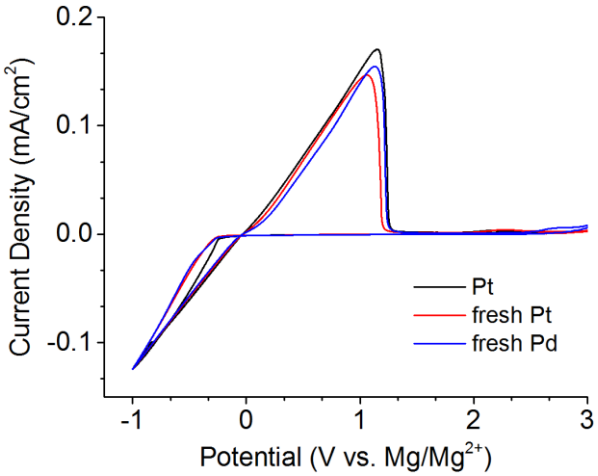


Figure 2.3: Cyclic voltammograms at 25 mV/s of the conditioned MACC in THF with different working electrodes: Pt used during conditioning (black), fresh Pt (red), and fresh Pd (blue).

2.3.2 SOLUTION COMPOSITION

To interrogate the effect of solution composition, the constituents of the MACC were systematically varied before and after conditioning. Figure 2.4 shows cyclic voltammograms obtained following the addition of 0.1 equivalents of $MgCl_2$ or $AlCl_3$ in THF to the conditioned MACC electrolyte. In a control experiment, the addition of THF alone did not significantly alter the electrochemistry (Figure 2.5). The addition of either $MgCl_2$ or $AlCl_3$ inhibits Mg deposition and stripping. For example, following the addition of $AlCl_3$ to the conditioned MACC, only 44% of the original stripping charge is present. Additionally, the data presented in Figure 2.4A show that the initial addition of $AlCl_3$ decreases the Coulombic efficiency from 97% to 83% and increases the overpotential from ~250 mV to ~450 mV. Similarly the addition of $MgCl_2$ decreases the Coulombic efficiency from 97% to 70% and increases the overpotential from ~250 mV to ~400 mV (Figure 2.4B). Interestingly, further cycling of the altered solutions restores the performance of the electrolytes to their original overpotentials and Coulombic efficiencies (Figure 2.4, blue). This finding means that the additional Mg or Al is accommodated in some

way during MACC conditioning and further suggests that the initial Mg:Al ratio may be altered during conditioning to achieve a consistent final value.

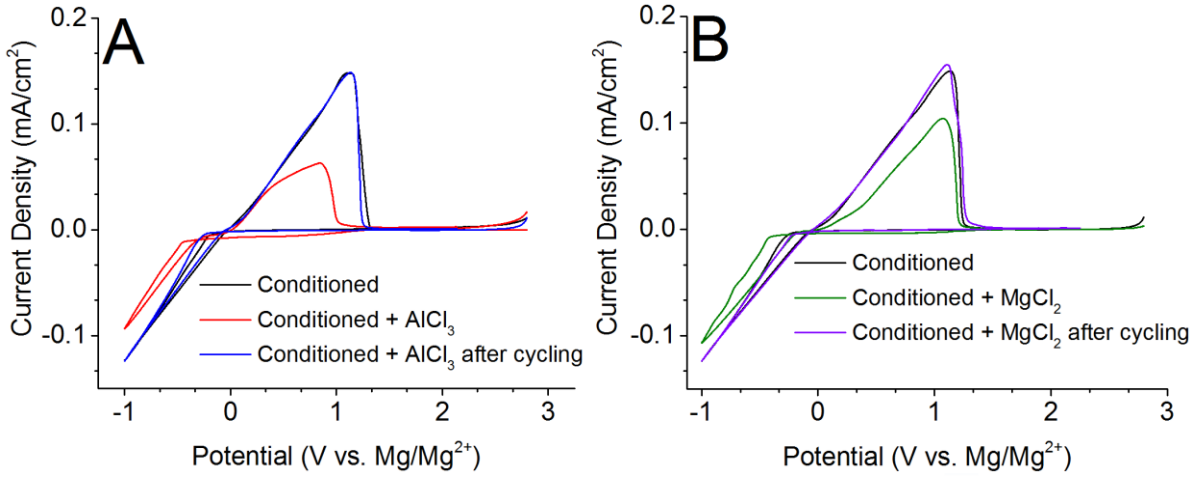


Figure 2.4: Cyclic voltammograms of conditioned MACC in THF (A and B, black), after adding 0.1 equivalents of $AlCl_3$ (A, red) and after conditioning of the altered solution (A, blue) and 0.1 equivalents of $MgCl_2$ (B, green), and after conditioning of the altered solution (B, purple) at 25 mV/s on Pt.

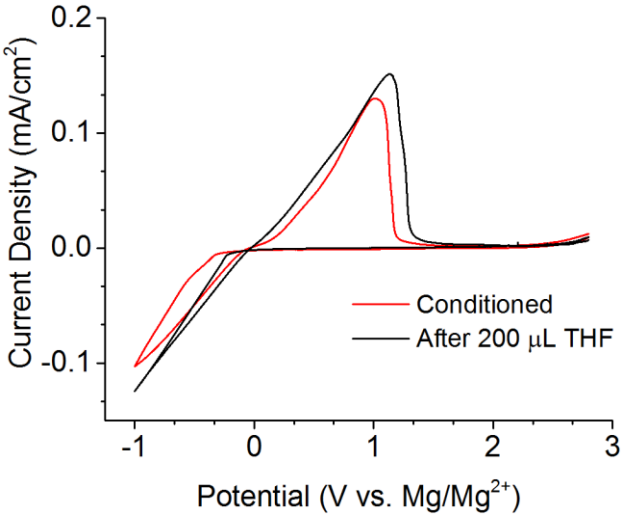


Figure 2.5: Cyclic voltammograms of the conditioned MACC in THF after adding 200 µL THF (black) and the same solution after conditioning (red).

Elemental analysis of the MACC solution was performed to determine how the conditioning process changes the electrolyte stoichiometry and if the solution reaches a converging Mg:Al ratio (Table 2.1). Regardless of the initial Mg:Al composition, freshly

synthesized solutions do not exhibit reversible Mg deposition. Upon cycling, however, Mg:Al electrolytes with 1:1 and 2:1 ratios demonstrate reversible Mg deposition. In both cases, the composition reaches a (2.59 ± 0.08):1 Mg:Al ratio. This finding suggests that irreversible Al or Mg deposition occurs until the electrolyte achieves a favorable composition. A 3:1 Mg:Al MACC in THF was attempted but could not attain this nominal stoichiometry due to the poor solubility of $MgCl_2$ in THF. As a result, the synthesized ratio is (2.7 ± 0.1):1, which ostensibly is ideal for reversible Mg deposition. This solution, however, cannot be conditioned even after extensive cycling, and the Mg:Al ratio diverges to 3.5:1. We propose that irreversible Mg and Al deposits must form during the early stages of conditioning. Here this initial irreversiblility causes the relative amount of Mg to increase beyond the necessary ~2.6:1 Mg:Al ratio.

Table 2.1: Summary of voltammetry and Mg:Al compositions of MACC electrolytes in THF as found by elemental analysis.

Nominal Molar Mg:Al Ratio	Sample	Found Molar Mg:Al Ratio	Coulombic Efficiency
1:1	Freshly synthesized	(0.98 ± 0.01):1	16%
	Conditioned	(2.6 ± 0.1):1	(99.8 ± 0.3)%
2:1	Freshly synthesized	(1.9 ± 0.2):1	14%
	Conditioned	(2.58 ± 0.06):1	(99.9 ± 0.2)%
3:1	Freshly synthesized	(2.7 ± 0.1):1	13%
	After 800 cycles	3.5:1	0%

The ~2.6:1 Mg:Al ratio for the conditioned MACC differs from that found in the crystallized electrolyte, $[Mg_2(\mu\text{-}Cl)_3\text{-}6THF][AlCl_4]$, where a 2:1 Mg:Al ratio was suggested.[12] Based on the elemental analysis reported above, it is likely the case that the crystallized electrolyte does not reflect the total composition of the solution nor the electroactive species. In-situ studies on similar Mg electrolytes recently demonstrated that interfacial species are not limited to dimers.[16] In particular recent X-ray studies propose that interfacial intermediates,

which do not contain Al, form during Mg deposition. We add to this picture by suggesting that the bulk electrolyte also contains excess Mg relative to the 2:1 Mg:Al ratio.

2.3.3 ELECTRODE MORPHOLOGY AND COMPOSITION

Since the composition of the electrolyte changes during conditioning, we expect that the excess Al or Mg initially present in the electrolyte deposits irreversibly on the working electrode surface. Figure 2.6 shows SEM-EDS data obtained from a Pt electrode after the last stripping cycle of MACC conditioning. Irregular deposits develop on the electrode, ones that are different from the bare surface of a fresh wire immersed in the conditioned MACC at OCP. EDS data show the presence of substantial Al, Mg, and Cl on the electrode, which is likely a consequence of irreversible deposition during conditioning.

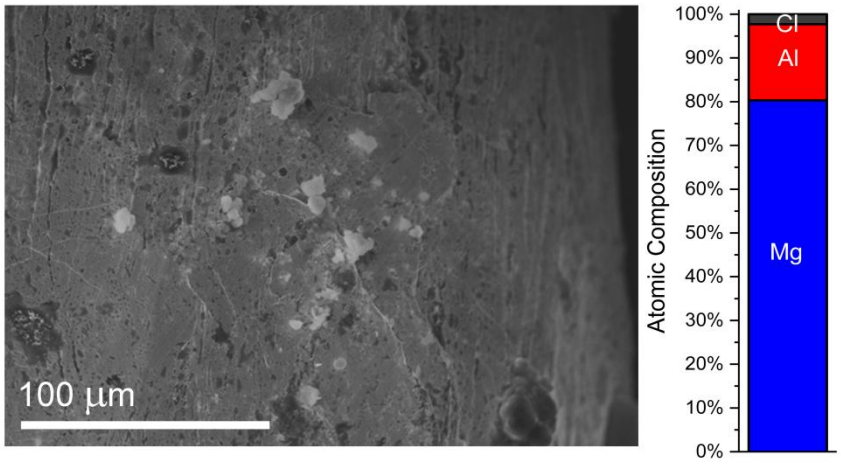


Figure 2.6: SEM-EDS data of a Pt surface used to condition the MACC in THF after the last stripping cycle. The graph on the right shows the relative percentages of Mg, Al, and Cl as determined by EDS from this sample.

To understand more fully the evolution of the electrolyte during conditioning, three representative stages were investigated (Figure 2.7A). After conditioning the MACC to each regime, a galvanostatic deposition of 30 mC of material onto a fresh Pt surface was performed. The fresh surface had never been used for MACC conditioning (Figure 2.8). This procedure

allowed us to analyze the nature of the electrodeposits at different conditioning stages regardless of conditioning history. As the MACC electrolyte evolves from the ~2:1 Mg:Al ratio initially present to the ~2.6:1 ratio found after conditioning, the morphology of the deposits transitions from discontinuous clumps to platelets, and Al codeposition diminishes (Figure 2.7B-D). These measurements show that Al codeposition from the conditioned MACC is inhibited relative to the unconditioned electrolyte.

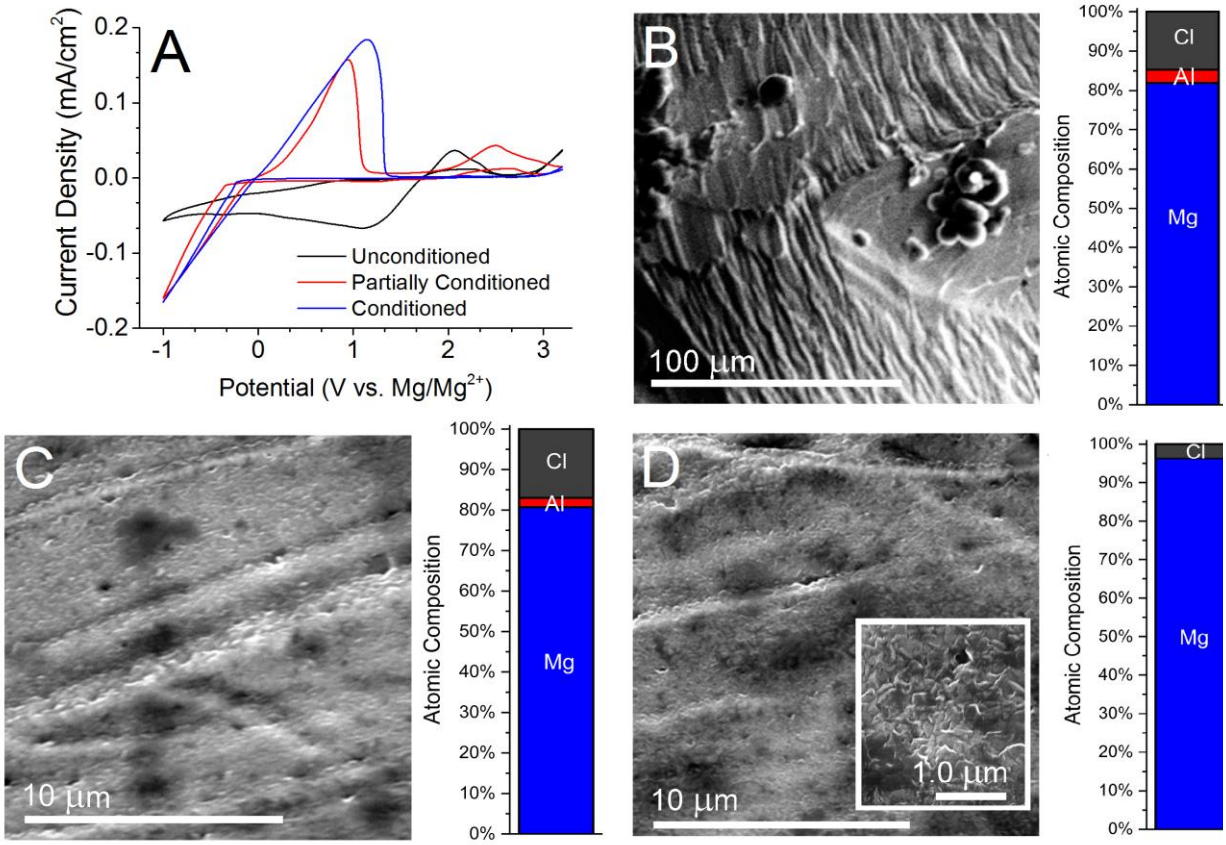


Figure 2.7: Cyclic voltammograms of the unconditioned (black), partially conditioned (red), and conditioned (blue) MACC in THF at 25 mV/s on Pt (A). SEM-EDS data of electrodeposits on fresh Pt surfaces (with relative percentages of Mg, Al, and Cl shown in the bar graphs) using the unconditioned (B), partially conditioned (C), and conditioned MACC (D).

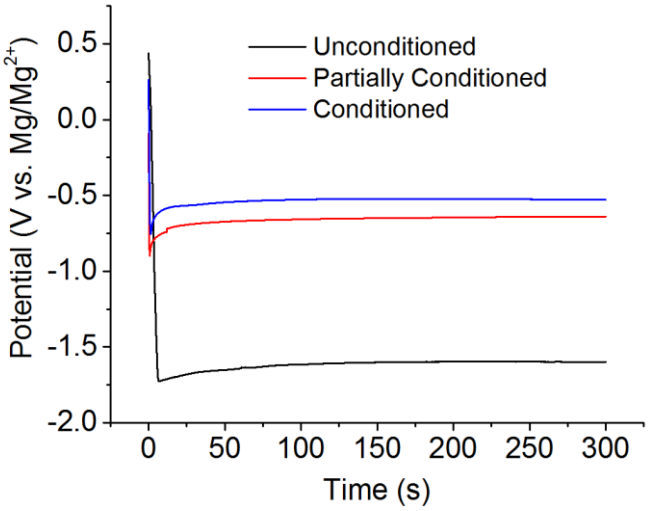


Figure 2.8: Chronopotentiometry of the unconditioned (black), partially conditioned (red), and conditioned (blue) MACC in THF at 100 μA/cm^2 on fresh Pt electrodes.

2.3.4 MACC AGING

Since the composition of the MACC changes during conditioning, its stability under resting conditions was investigated. Figure 2.9 shows cyclic voltammograms obtained immediately following conditioning and after allowing the electrolyte to rest in a sealed cell in the glove box for one week at open circuit potential. The aged electrolyte exhibits a substantially greater overpotential for deposition (~500 mV vs. ~200 mV for the conditioned MACC), a diminished Mg stripping peak, and a Coulombic efficiency that diminished by ~35%. This aging effect was observed regardless of the conditioning method or working electrodes used (Figure 2.10). Interestingly, if we condition the aged electrolyte by cycling as previously described, the performance is recovered of the conditioned electrolyte.

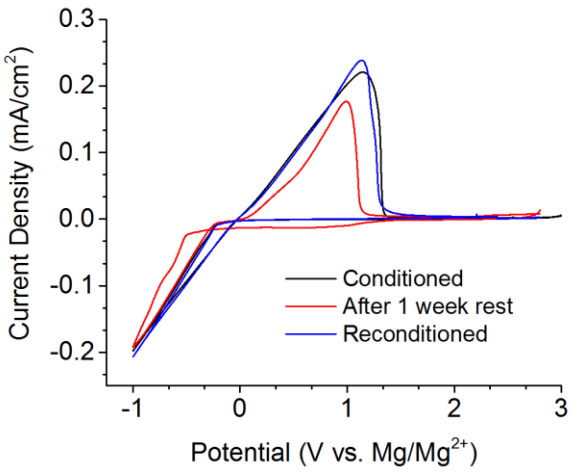


Figure 2.9: Cyclic voltammograms of the freshly conditioned MACC in THF (black), after resting for one week at OCP (red), and after reconditioning (blue).

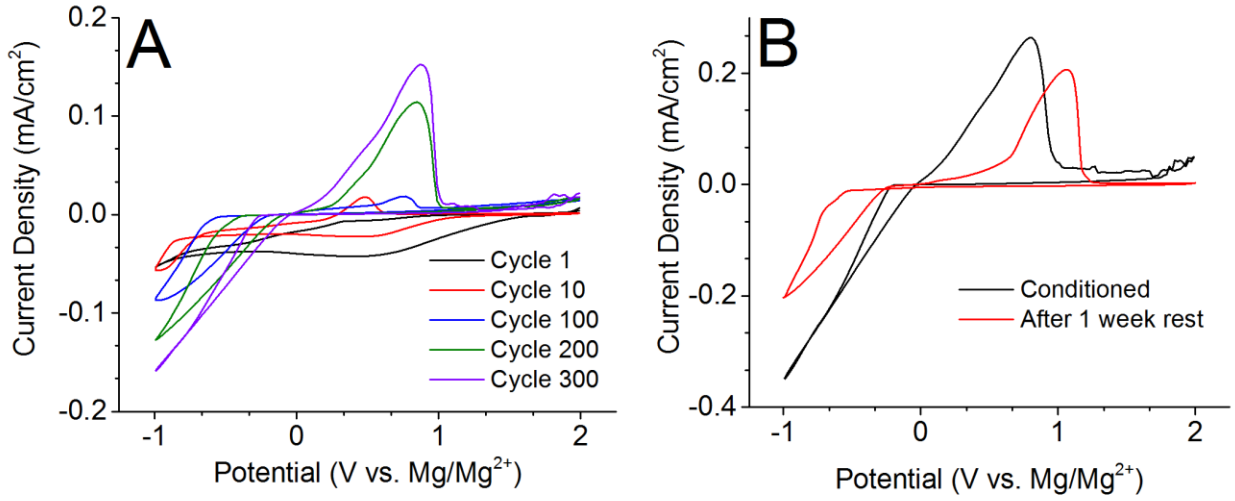


Figure 2.10: Cyclic voltammograms of cycle 1 (black), cycle 10 (red), cycle 100 (blue), cycle 200 (green), cycle 300 (purple) of the MACC in THF at 25 mV/s on a Pt electrode (A). Cyclic voltammograms of the freshly conditioned MACC in THF (black) and after resting for one week at OCP (red) (B).

2.3.5 MS STUDIES

The conditioning and aging measurements demonstrate that the bulk composition of the electrolyte evolves with both time and cycling. To probe the composition of the MACC under these conditions, ESI-MS of the electrolyte was performed by introducing the MACC into the MS under an inert atmosphere.

ESI-MS studies show that the freshly synthesized MACC electrolyte contains high molecular weight ions with m/z values greater than 400 (Figure 2.11). These high molecular weight ions are ascribed to oligomeric complexes of THF. Tables 2.2 show families of oligomeric species associated with solvent decomposition found by ESI-MS. Interestingly, these oligomers are not present in the conditioned MACC in THF (Table 2.2, Table 2.3, Figure 2.11B). Thus we hypothesize that the conditioning process removes inhibitory THF oligomers from the electrolyte. Additionally, another decomposition product of THF was found, γ-butyrolactone (GBL), consistent with previous studies using $Mg(AlCl_2EtBu)_2$, which showed that this oxidation product of THF also formed upon cycling.[13] In the one-week-aged MACC in THF, ESI-MS analysis also shows that the electrolyte contains high molecular weight ions attributed to THF oligomers (Table 2.2, Table 2.5, Figure 2.11C). Therefore, the decrease in electrochemical performance of the aged MACC in THF is due to these oligomeric species.

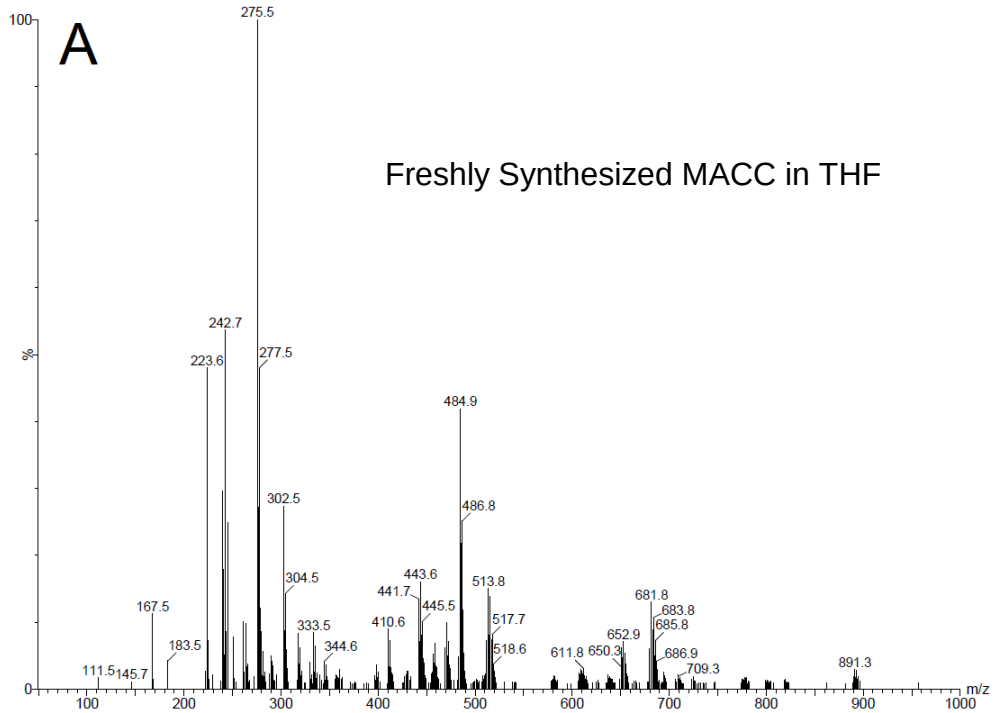
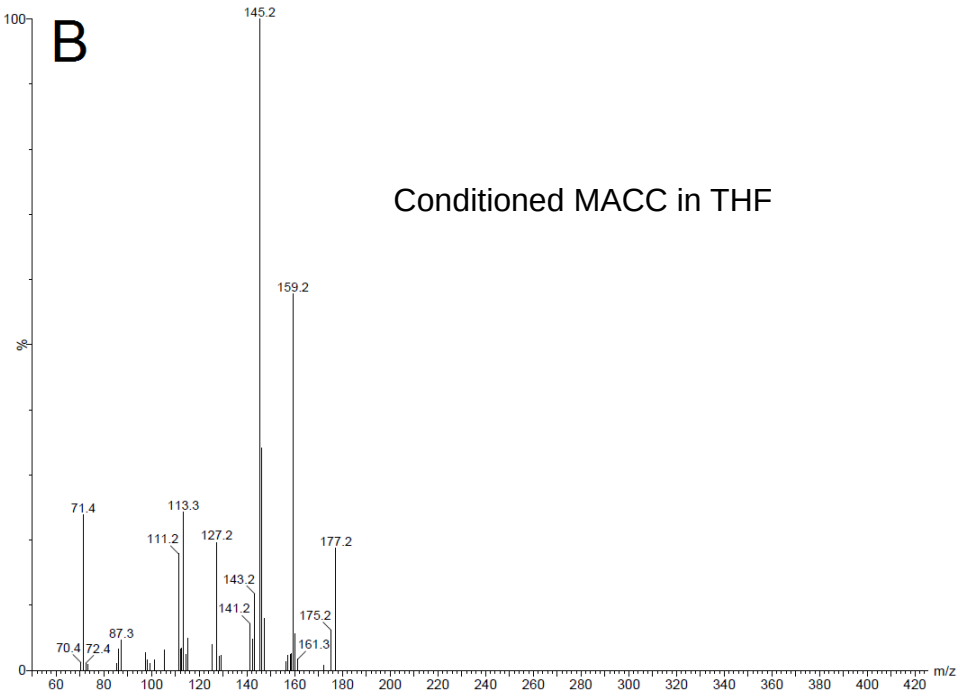


Figure 2.11 (cont.)



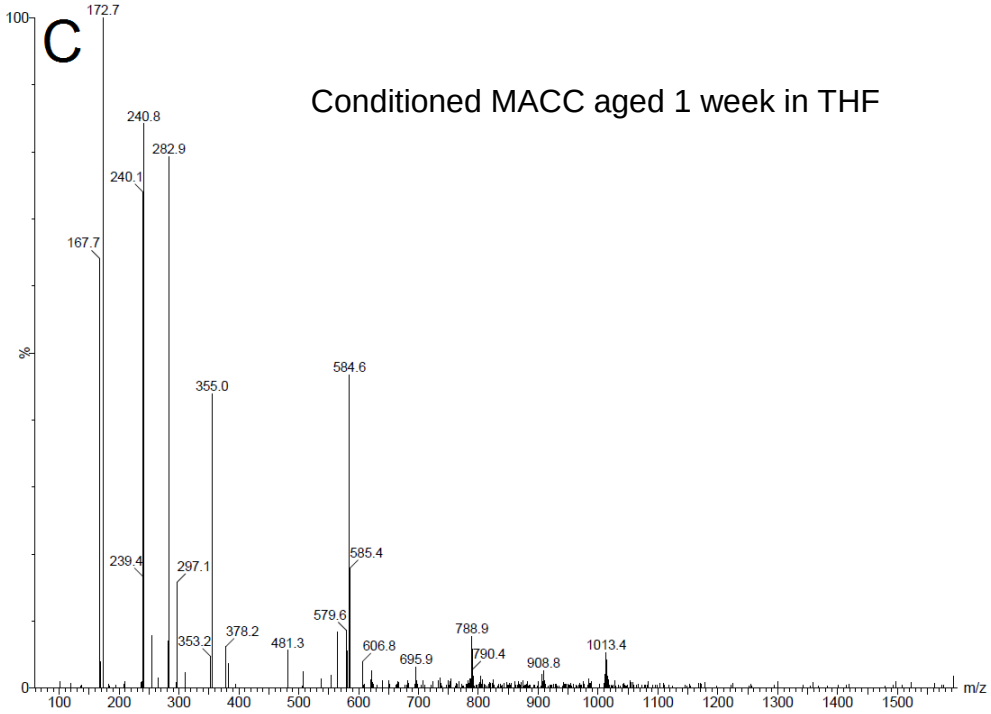


Figure 2.11 (cont.)

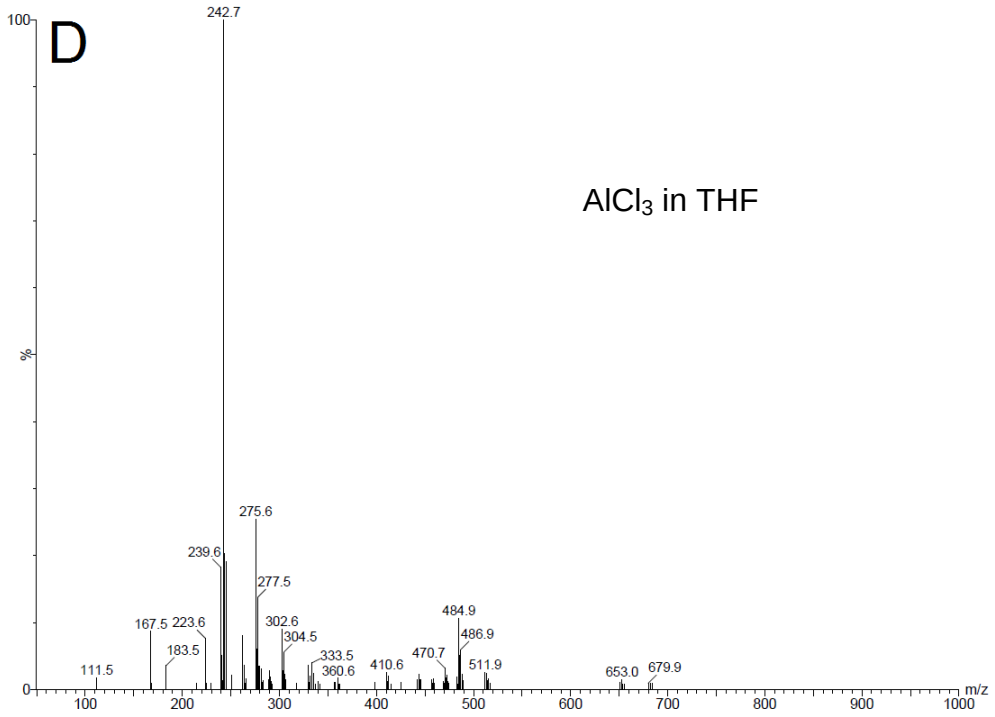


Figure 2.11: ESI-MS of the freshly synthesized MACC (A), conditioned MACC (B), conditioned MACC in THF aged one week (C), and a solution of $AlCl_3$ in THF (D).

Table 2.2: Representative solvent decomposition peaks as found by ESI-MS.

Sample	**m/z**	**Assignment**
Unconditioned MACC in THF	72n - 27 (n = 4, 5)	$[(THF)_n\text{-}C_2H_4+H]^+$
	72n - 43 (n = 9, 10)	$[(THF)_n\text{-}C_2H_4\text{-}CH_2+H]^+$
	72n + 149 (n = 7)	$[AlCl_3O(THF)_n\text{-}H_2+H]^+$
Conditioned MACC in THF	87	$[GBL+H]^+$
Conditioned MACC in THF after one week at OCP	72n - 27 (n = 13)	$[(THF)_n\text{-}C_2H_4+H]^+$
	72n - 43 (n = 9, 10)	$[(THF)_n\text{-}C_2H_4\text{-}CH_2+H]^+$
	72n + 149 (n = 12)	$[AlCl_3O(THF)_n\text{-}H_2+H]^+$
$AlCl_3$ in THF	72n - 27 (n = 4, 5)	$[(THF)_n\text{-}C_2H_4+H]^+$
	72n - 43 (n = 10)	$[(THF)_n\text{-}C_2H_4\text{-}CH_2+H]^+$
	72n + 149 (n = 7)	$[AlCl_3O(THF)_n\text{-}H_2+H]^+$

Table 2.3: Peak assignments for ESI-MS of the freshly synthesized MACC.

m/z	Assignment
113	$[AlCl(THF)_2\text{-}2C_2H_4\text{-}2H_2O\text{-}H]^+$
145	$[AlCl(THF)_2\text{-}C_2H_4\text{-}H_2O\text{-}CH_2\text{-}H]^+$
243	$[(THF)_4\text{-}C_2H_4\text{-}H_2O\text{+}H]^+$
261	$[(THF)_4\text{-}C_2H_4\text{+}H]^+$
275	$[(THF)_4\text{-}CH_2\text{+}H]^+$
302	$[(THF)_5\text{-}OCH_3\text{-}C_2H_4\text{-}H]^+$
330	$[(THF)_5\text{-}OCH_3\text{+}H]^+$
333	$[(THF)_5\text{-}C_2H_4\text{+}H]^+$
345	$[(THF)_5\text{-}CH_2\text{-}H_2\text{+}H]^+$
359	$[(THF)_5\text{-}H_2\text{+}H]^+$
361	$[(THF)_5\text{+}H]^+$
446	$[(THF)_7\text{-}OCH_3\text{-}C_2H_4\text{+}H]^+$
460	$[(THF)_7\text{-}OCH_3\text{-}CH_2\text{+}H]^+$
487	$[(THF)_7\text{-}H_2O\text{+}H]^+$
518	$[(THF)_8\text{-}OCH_3\text{-}C_2H_4\text{-}H]^+$
607	$[(THF)_9\text{-}C_2H_4\text{-}CH_2\text{+}H]^+$
653	$[AlCl_3O(THF)_7\text{-}H_2\text{+}H]^+$
680	$[(THF)_{10}\text{-}C_2H_4\text{-}CH_2\text{+}H]^+$
708	$[(THF)_{10}\text{-}CH_2\text{+}H]^+$
891	$[(THF)_{13}\text{-}H_2O\text{-}C_2H_4\text{+}H]^+$

Table 2.4: Peak assignments for ESI-MS of the conditioned MACC in THF.

m/z	Assignment
87	$[GBL\text{+}H]^+$
97	$AlCl_2^+$
105	$[MgCl_2(THF)\text{-}C_2H_4\text{-}H_2O\text{-}CH_2]^+$
113	$[AlCl(THF)_2\text{-}2C_2H_4\text{-}2H_2O\text{-}H]^+$
127	$[AlCl(THF)_2\text{-}C_2H_4\text{-}2H_2O\text{-}CH_2\text{-}H]^+$
145	$[AlCl(THF)_2\text{-}C_2H_4\text{-}H_2O\text{-}CH_2\text{-}H]^+$
159	$[AlCl(THF)_2\text{-}C_2H_4\text{-}H_2O\text{-}H]^+$
177	$[AlCl(THF)_2\text{-}C_2H_4\text{-}H]^+$

Table 2.5: Peak assignments for ESI-MS of the conditioned MACC in THF aged one week.

m/z	Assignment
241	$[(THF)_4\text{-}C_2H_4\text{-}H_2O\text{-}H_2+H]^+$
283	$[Mg(THF)_4\text{-}C_2H_4\text{-}H]^+$
297	$[Mg_2Cl_3(THF)_2]^+$
355	$[MgCl_2(THF)_4\text{-}C_2H_4+H]^+$
379	$[AlCl_3O(THF)_4\text{-}C_2H_4\text{-}CH_2+H]^+$
585	$[Mg_2Cl_3(THF)_6]^+$
607	$[(THF)_9\text{-}C_2H_4\text{-}CH_2+H]^+$
680	$[(THF)_{10}\text{-}C_2H_4\text{-}CH_2+H]^+$
696	$[(THF)_9\text{-}C_2H_4+H]^+$
737	$[Mg_2Cl_2(THF)_9\text{-}C_2H_4\text{-}H]^+$
754	$[AlCl(THF)_{10}\text{-}C_2H_4\text{-}H]^+$
789	$[AlCl_2(THF)_{10}\text{-}C_2H_4]^+$
826	$[AlCl(THF)_{11}\text{-}C_2H_4\text{-}H]^+$
907	$[(THF)_{13}\text{-}C_2H_4\text{-}H_2+H]^+$
909	$[(THF)_{13}\text{-}C_2H_4+H]^+$
1014	$[AlCl_3O(THF)_{12}\text{-}H_2+H]^+$
1053	$[Mg_2Cl_2(THF)_{13}\text{-}H]^+$

Table 2.6: Peak assignments for ESI-MS of a solution of $AlCl_3$ in THF

m/z	Assignment
215	$[(THF)_3\text{-}H_2+H]^+$
243	$[(THF)_4\text{-}C_2H_4\text{-}H_2O+H]^+$
261	$[(THF)_4\text{-}C_2H_4+H]^+$
275	$[(THF)_4\text{-}CH_2+H]^+$
287	$[(THF)_4\text{-}H_2+H]^+$
289	$[(THF)_4+H]^+$
302	$[(THF)_5\text{-}\ OCH_3\text{-}C_2H_4\text{-}H]^+$
330	$[(THF)_5\text{-}OCH_3+H]^+$
333	$[(THF)_5\text{-}C_2H_4+H]^+$
359	$[(THF)_5\text{-}H_2+H]^+$
361	$[(THF)_5+H]^+$
446	$[(THF)_7\text{-}\ OCH_3\text{-}C_2H_4\text{-}H]^+$
459	$[(THF)_7\text{-}H_2O+H]^+$
487	$[(THF)_7\text{-}C_2H_4\text{-}H_2O+H]^+$
518	$[(THF)_8\text{-}\ OCH_3\text{-}C_2H_4\text{-}H]^+$
653	$[AlCl_3O(THF)_7\text{-}H_2+H]^+$
680	$[(THF)_{10}\text{-}C_2H_4\text{-}CH_2+H]^+$

The detection of oligomeric THF species in the unconditioned and aged MACC prompted us to consider the mechanism of THF oligomerization in these systems. Previous studies have demonstrated that $AlCl_3$ acts as a Lewis acid catalyst to ring-open polymerize THF.[17] ESI-MS

analysis was performed on solutions of $AlCl_3$ in THF and find that these also contain oligomers (Table 2.2 Table 2.6, Figure 2.11D). In addition, some of our observations during the synthesis procedure are possibly explained by the presence of THF oligomers. We find that careful, slow, and cold addition of $AlCl_3$ to THF produces MACC solutions that are more rapidly conditioned than ones prepared at room temperature. The addition of $AlCl_3$ to THF is very exothermic, and we hypothesize that the cold addition minimizes oligomer formation.

2.3.6 ADDITION OF POLY-THF

To explore the inhibition of MACC by multimeric THF species further, polyTHF was added to the conditioned MACC. Figure 2.12 shows that the deposition overpotential of the MACC electrolyte with added polyTHF increases to ~550 mV from ~200 mV, and the Coulombic efficiency decreases by ~50%. These findings illustrate that the performance of the MACC significantly decreases due to the addition of polyTHF. Upon cycling, however, the efficiency and overpotential are restored to the conditioned values (Figure 2.12, blue). This result further supports the hypothesis that multimeric THF species inhibit performance and suggests that conditioning removes these species.

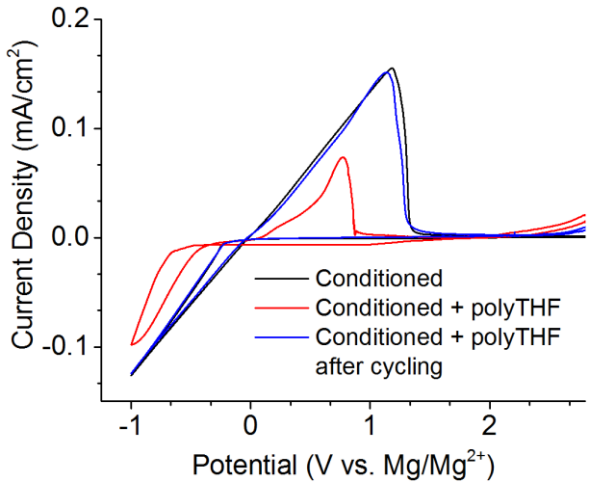


Figure 2.12: Cyclic voltammograms of the conditioned MACC in THF (black), the conditioned MACC with 0.5 wt. % polyTHF added (red), and the reconditioned MACC with 0.5 wt. % polyTHF added (blue).

2.3.7 MACC IN DME

Because ring-opening polymerization inhibits the performance of the MACC in THF under resting conditions, the MACC was prepared in an acyclic ether solvent, DME. Figure 2.13A shows that the MACC in DME requires a similar conditioning process to the MACC in THF to reversibly deposit and strip Mg. Once the MACC in DME is conditioned, the overpotential for Mg deposition is ~150 mV, and the Coulombic efficiency is 92% (Figure 2.13B, black). Unlike the MACC in THF, the performance of the MACC in DME does not change as dramatically after one week of rest at OCP. The overpotential before and after resting remains the same, and the Coulombic efficiency decreases by ~10% in contrast to the ~35% decrease observed in THF. The improved resting stability in DME is likely associated with the inability of DME to ring-open polymerize. ESI-MS confirms that no oligomeric species are present at any conditioning stage of the MACC in DME (Table 2.7, Figure 2.14). As with the MACC in THF, conditioning establishes a favorable Mg:Al ratio of ~2.6:1. While no solvent decomposition is detectable for the MACC in DME, the Coulombic efficiency plateaus at ~92%

instead of the ~100% efficiency obtained with the MACC in THF (Figure 2.15). The origin of this behavior is not completely understood at present, but it seems likely that it must relate to the speciation and structures of Mg:Al complexes present in this solvent.

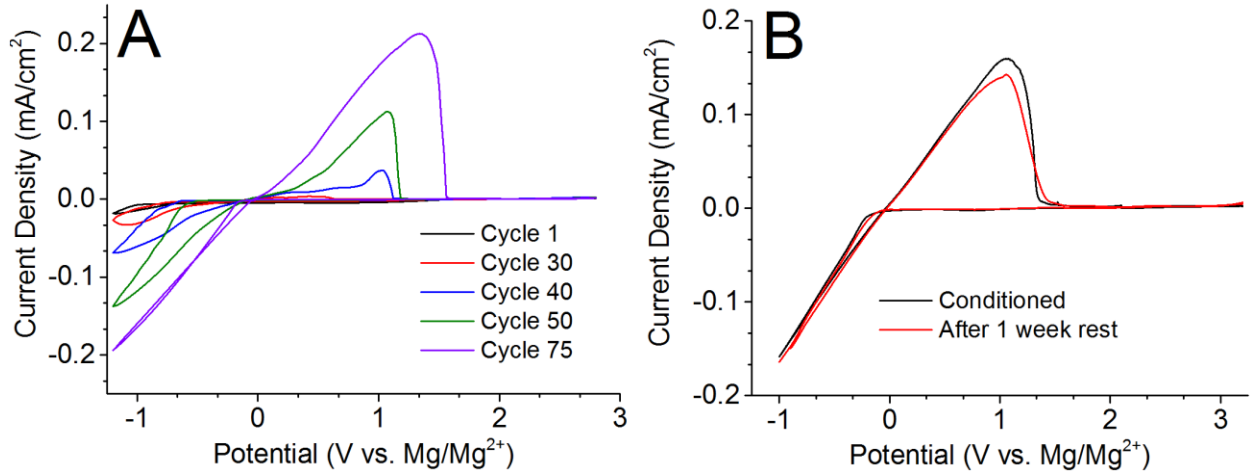


Figure 2.13: Cyclic voltammograms of cycle 1 (black), cycle 30 (red), cycle 40 (blue), cycle 50 (green), cycle 75 (purple) of the MACC in DME at 5 mV/s on a Pt electrode (A). Cyclic voltammograms of the conditioned MACC in DME (black) and after resting for one week at OCP (red) (B).

Table 2.7: Peak assignments for ESI-MS of the MACC in DME. Note that the ESI-MS was performed in THF since DME peaks obscured analysis.

m/z	**Assignment**
119	$[Mg_2Cl_2+H]^+$
139	$[Mg(THF)_2\text{-}C_2H_4\text{-}H]^+$
175	$[MgCl(THF)_2\text{-}C_2H_4]^+$
231	$[AlCl(THF)_3\text{-}C_2H_4\text{-}H_2O\text{-}H]^+$
239	$[MgCl_2(THF)_2+H]^+$
249	$[AlCl(THF)_3\text{-}C_2H_4\text{-}H]^+$
283	$[MgCl_2(THF)_3\text{-}C_2H_4+H]^+$
323	$[Mg_2Cl_3(THF)_3\text{-}C_2H_4\text{-}H_2O]$
407	$[Mg_2Cl_2(THF)_4+H]^+$

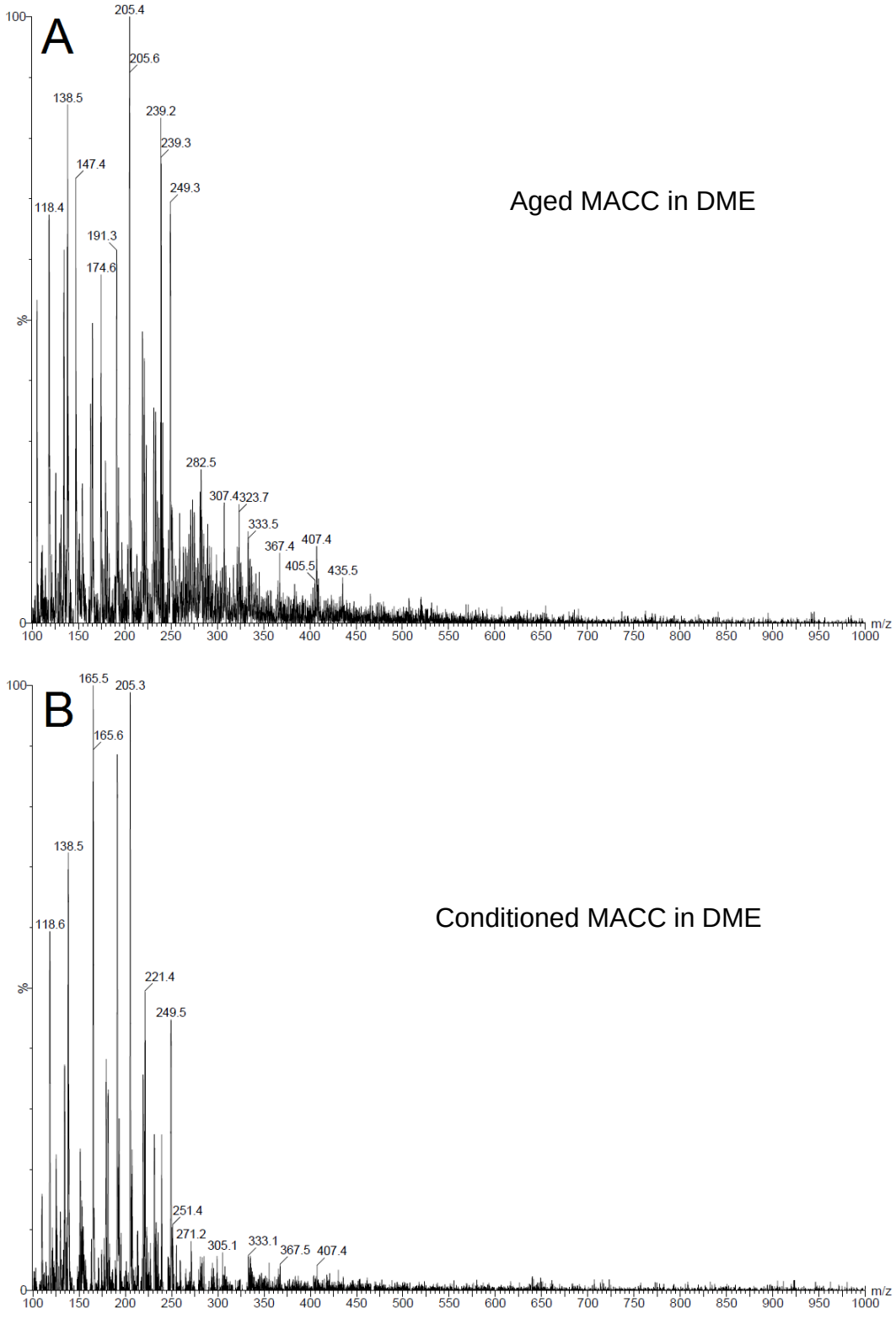


Figure 2.14 (cont.)

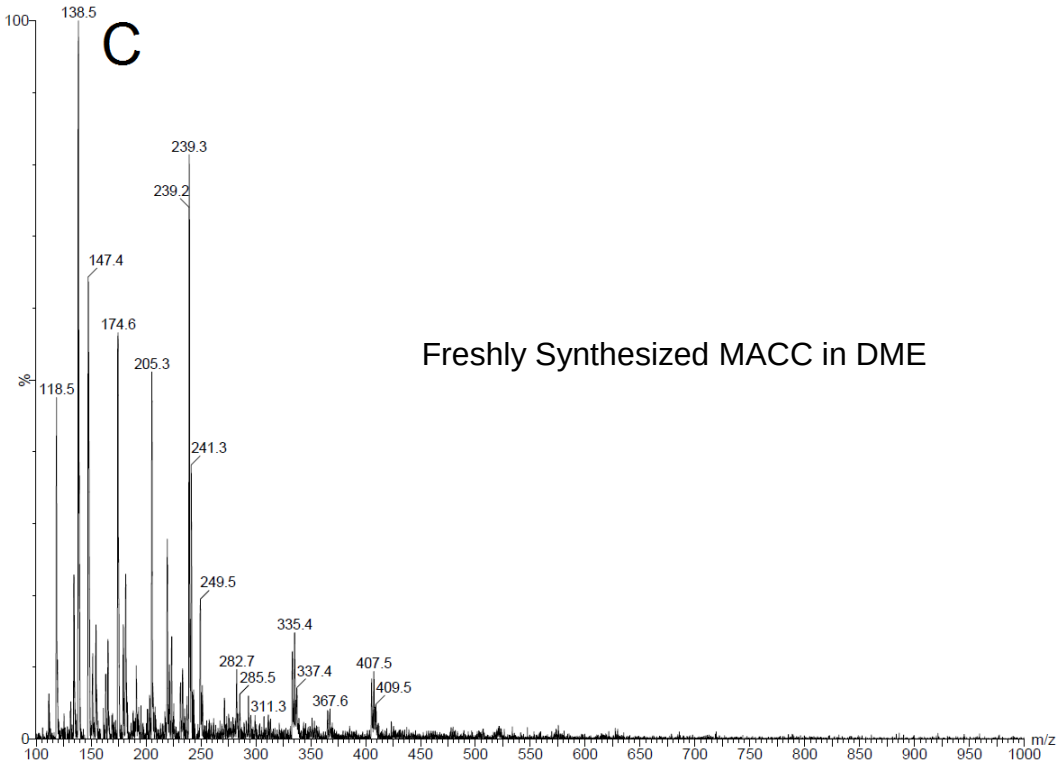


Figure 2.14: ESI-MS of the MACC in DME aged one week (A), conditioned (B), and freshly synthesized (C).

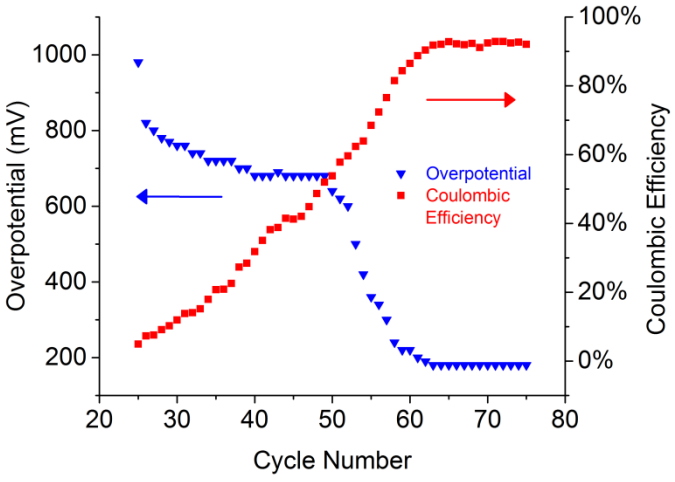


Figure 2.15: Mg deposition overpotential and Coulombic efficiency as a function of cycle number obtained from cyclic voltammetry of the MACC in DME at 5 mV/s on a Pt electrode.

2.3.8 PROPOSED MECHANISM IN THF

From our experimental findings and previous literature describing the speciation of Mg and Al chlorides in THF, a mechanism for Mg deposition from the conditioned MACC in THF was proposed. Since the conditioned MACC has a Mg:Al composition of ~2.6:1, Mg electrodeposition cannot be fully explained by a dimeric Mg complex, which contains a 2:1 Mg:Al ratio. Regardless, the crystallized MACC possesses a dimeric structure, indicating that dimeric Mg is a thermodynamically favorable species.[12] The ~2.6:1 Mg:Al composition in the conditioned MACC may be explained by an equilibrium mixture of dimeric and trimeric Mg species (Figure 2.16, a). Indeed, in addition to dimers, Mg chloride trimers have previously been crystallized from ethereal solutions.[18,19] Recent X-ray studies in electrolytes similar to the MACC have shown that monomeric Mg species exist at the surface during Mg electrodeposition.[16] Assuming these findings are also applicable to the MACC system, we propose that a trimeric Mg chloride complex approaches the surface and breaks into a dimer and a monomer (Figure 2.17, b) from which Mg subsequently deposits. The proposed trimer-dimer equilibrium allows the bulk composition of the electrolyte to exist in thermodynamically favorable multimeric forms throughout Mg deposition.

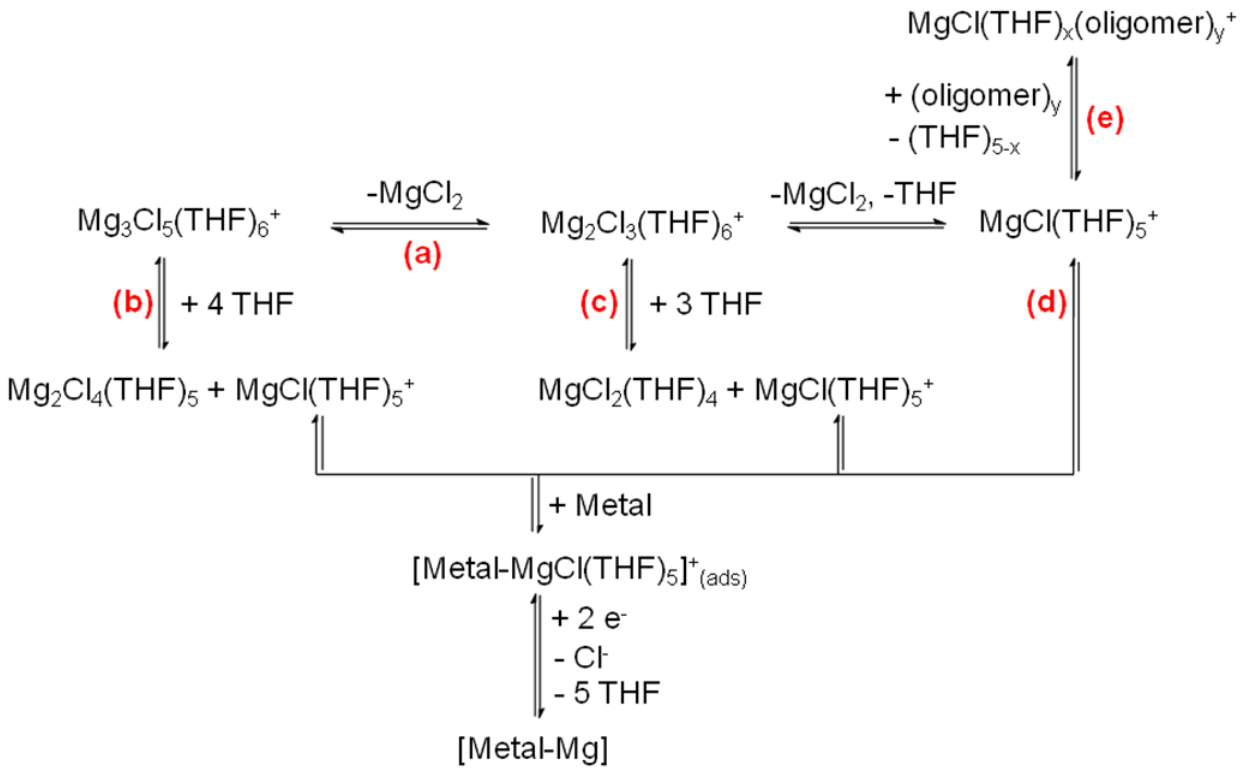


Figure 2.16: Possible pathways for Mg deposition from the MACC in THF. Equilibrium between trimeric and dimeric Mg complexes (a). Mg deposition from a trimer (b), dimer (c), and monomer (d). Equilibrium involving THF oligomers (e).

We hypothesize that by altering the Mg:Al stoichiometry, the conditioning process shifts the equilibrium composition of the MACC electrolyte so that it contains species that support reversible Mg deposition and stripping. In the early stages of the conditioning process, Mg deposition occurs at high overpotentials, possibly from dimeric or monomeric species (Figure 2.16, c and d). The large overpotentials for these processes likely reflect the fact that these pathways generate thermodynamically unfavorable monomeric species upon deposition. Additionally, Al deposition occurs during the conditioning process, which may originate from Al cationic species. Conditioning the MACC solution alters the Al speciation in the electrolyte to predominantly $AlCl_4^-$. Previous studies have shown that Al electrodeposition from THF solutions containing $AlCl_4^-$ occurs less readily than from solutions containing cationic Al species.[20]

Similarly, in the MACC system, Al deposition is minimized once Al species are kinetically protected from deposition in the form of anions. Therefore, we hypothesize that reversible Mg deposition occurs from the conditioned MACC in THF via multimeric homometallic Mg complexes.

From this mechanistic picture, we rationalize the detrimental effect that THF oligomers have on the electrochemical performance of the MACC in THF. The multidentate nature of THF oligomers causes them to act as chelating agents. Since chelators preferentially bind monometallic centers, we expect the THF oligomers to shift the Mg equilibria towards monomeric forms (Figure 2.16, e).[21] As previously stated, deposition from monomeric Mg species is thermodynamically unfavorable. This speciation towards monomers causes the large overpotential measured in the aged MACC in THF.

2.3.9 TEMPERATURE STUDIES

Having established a mechanistic framework for Mg deposition and stripping from the MACC in THF, we decided to analyze the effect of temperature on the conditioning process. Given the complexity of the system, numerous enthalpic, entropic, and kinetic parameters must be considered to predict the relationship between temperature and electrochemical behavior. Our work suggests that multimeric Mg species are more thermodynamically stable in bulk solution than monomeric Mg species. Monomeric species, however, are entropically favored because their bulk solutions are more disordered than solutions containing multimeric species. From the Gibbs free energy equation, we expect therefore that multimeric Mg species are more stable from an enthalpic perspective. This enthalpic stability is in keeping with the anticipated more favorable heat of formation associated with the additional bridging bonds present in multimeric

complexes. From these considerations, higher temperatures would favor monomeric species, resulting in decreased performance.

This thermodynamic prediction, however, does not account for the kinetics of equilibria dynamics. At higher temperatures, the exchange rates between multimeric and monomeric species are likely faster, allowing multimeric Mg species to be accessed more readily. Since Mg deposition from multimeric species is more facile, conditioning at higher temperatures would allow reversible Mg deposition to occur more readily due to the increased equilibria exchange rates. Because thermodynamic and kinetic arguments predict different outcomes, the electrochemical dependence on temperature may give insight into the kinetic and thermodynamic controls of the MACC conditioning process. We note that the kinetics and energetics of all species in solution, including Al and oligomeric species, will also likely be affected by temperature changes.

We performed experiments testing the MACC conditioning process at more extreme conditions with bulk solution temperatures at 5 ºC, 25 ºC, and 40 ºC and an expanded electrochemical cycling window. Because Mg deposition at 5 ºC was significantly inhibited, we cycled the working electrodes to more positive and negative potentials (3.2 V to -1.8 V vs. Mg/Mg^{2+}) in an attempt to aid the conditioning process. We found that temperature significantly impacted the electrochemical conditioning. Figure 2.17A shows cyclic voltammograms of the freshly synthesized MACC in THF at cycle 25 of the conditioning process at 5 ºC, 25 ºC, and 40 ºC. The electrochemical performance of electrolytes at higher temperatures improved faster than those at lower temperatures during the first 25 cycles (Figures 2.17B and 2.17C). In particular, at cycle 25, the Mg deposition overpotential for the MACC in THF at 40 ºC is ~200 mV while the overpotential at 25 ºC is ~270 mV (Figure 2.17B). In contrast, the MACC in THF at 5 ºC showed

highly irreversible behavior throughout most of the conditioning process. Figure 2.17C shows the Coulombic efficiencies of the MACC at the three temperatures studied as a function of cycle number. The Coulombic efficiency of the MACC conditioned at 40 ºC begins to increase earlier than the MACC conditioned at 25 ºC. The MACC cycled at 5 ºC does not display any anodic Mg stripping features during the first 25 cycles.

The results from these studies demonstrate that higher temperatures expedite the early stages of the conditioning of the MACC in THF. These findings suggest that the initial conditioning process is controlled by the kinetics of trimer-dimer-monomer equilibria and are not as dependent on the thermodynamic parameters of Mg species. Future studies will more thoroughly investigate the effect of temperature on the MACC conditioning and aging process. Additionally, few thermodynamic and kinetic parameters have been quantitated here, but future computational studies may give more insight into the Mg deposition and stripping process of the MACC.

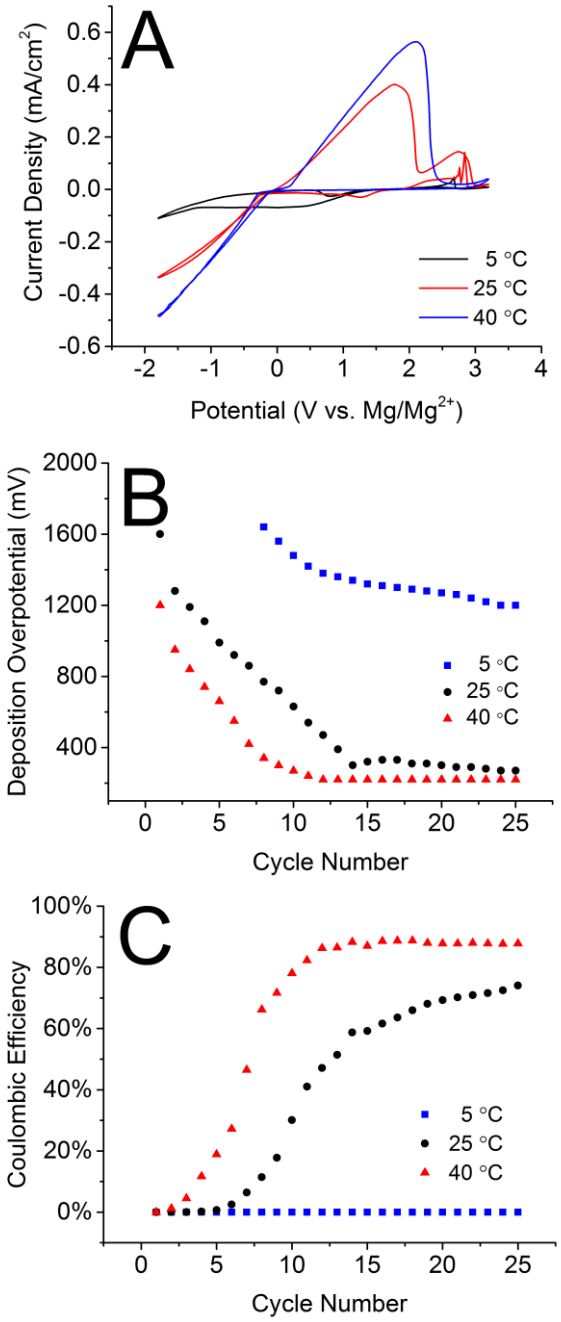


Figure 2.17: Cyclic voltammograms of the conditioning process of the MACC in THF at 5 mV/s on a Pt electrode (working area of ~1.2 cm^2) at 5 ºC (blue), 25 ºC (black), and 40 ºC (red). Cycle 25 for each temperature is shown (A). Mg deposition overpotential (B) and Coulombic efficiency (C) as a function of cycle number at 5 ºC (blue), 25 ºC (black), and 40 ºC (red).

2.4 CONCLUSIONS

The electrochemistry and composition of MACC systems was analyzed, showing that reversible Mg deposition occurs after substantial electrochemical conditioning. SEM-EDS and elemental analysis show that Mg and Al irreversibly deposit until the electrolyte attains an ideal Mg:Al stoichiometry of ~2.6:1. ESI-MS data reveal that oligomeric THF species are formed during synthesis and after aging. The conditioning process may improve the performance of the MACC by both adjusting the solution composition to a favorable Mg:Al stoichiometry and temporarily ridding the solution of inhibitory THF oligomers. From these results, we propose that speciation favoring multimeric homometallic Mg complexes enables reversible Mg deposition from the conditioned MACC in THF. The conditioned MACC electrolyte demonstrates reversible Mg deposition and a large electrochemical window, characteristics that are necessary for practical Mg-ion batteries. However, this study illustrates that acyclic solvents may be required to avoid unwanted aging processes, which would severely limit the shelf life of a useful battery.

2.5 REFERENCES

1. Yoo, H.; Shterenberg, I.; Gofer, Y.; Gershinsky, G.; Pour, N.; Aurbach, D. Mg Rechargeable Batteries: An On-Going Challenge. *Energy Environ. Sci.*, **2013**, *6*, 2265-2279.

2. Yoshio, M.; Brodd, R.; Kozawa, A. *Lithium-Ion Batteries: Science and Technologies*; Springer Publishing: New York, NY, 2009.

3. Aurbach, D.; Gofer, Y.; Lu, Z.; Schechter, A.; Chusid, O.; Gizbar, H.; Cohen, Y.; Ashkenazi, V.; Moshkovich, M.; Turgeman, R.; Levi, E. A Short Review on the Comparison Between Li Battery Systems and Rechargeable Magnesium Battery Technology. *J. Power Sources*, **2001**, *97*, 28-32.

4. Saha, P.; Datta, M.; Velikokhatnyi, O.; Manivannan, A.; Alman, D.; Kumta, P. Rechargeable Magnesium Battery: Current Status and Key Challenges for the Future. *Prog. Mater. Sci.*, **2014**, *66*, 1-86.

5. Burns, J.; Kassam, A.; Sinha, N.; Downie, L.; Solnickova, L.; Way, B.; Dahn, J. Predicting and Extending the Lifetime of Li-Ion Batteries. *J. Electrochem. Soc.*, **2013**, *160*, A1451-A1456.

6. Bond, T.; Burns, J.; Stevens, D.; Dahn, H.; Dahn, J. Improving Precision and Accuracy in Coulombic Efficiency. *J. Electrochem. Soc.*, **2013**, *160*, A521-A527.

7. Gregory, T.; Hoffman, R.; Winterton, R. Nonaqueous Electrochemistry of Magnesium: Applications to Energy Storage. *J. Electrochem. Soc.*, **1990**, *137*, 775-780.

8. Aurbach, D.; Moshkovich, M.; Schechter, A.; Turgeman, R. Magnesium Deposition and Dissolution Processes in Ethereal Grignard Salt Solutions using Simultaneous EQCM-EIS and In Situ FTIR Spectroscopy. *Electrochem. Solid State*, **2000**, *3*, 31-34.

9. Aurbach, D.; Lu, Z.; Schechter, A.; Gofer, Y.; Gizbar, H.; Turgeman, R.; Cohen, Y.; Moshkovich, M.; Levi, E. Prototype Systems for Rechargeable Magnesium Batteries. *Nature*, **2000**, *407*, 724-727.

10. Mizrahi, O.; Amir, N.; Pollak, E.; Chusid, O.; Marks, V.; Gottlieb, H.; Larush, L.; Zinigrad, E.; Aurbach, D. Electrolyte Solutions with a Wide Electrochemical Window for Rechargeable Magnesium Batteries. *J. Electrochem. Soc.*, **2008**, *155*, A103-A109.

11. Doe, R.; Han, R.; Hwang, J.; Gmitter, A.; Shterenberg, I.; Yoo, H.; Pour, N.; Aurbach, D. Novel, Electrolyte Solutions Comprising Fully Inorganic Salts with High Anodic Stability for Rechargeable Magnesium Batteries. *Chem. Commun.*, **2014**, *50*, 243-245.

12. Liu, T.; Shao, Y.; Li, G.; Gu, M.; Hu, J.; Xu, S.; Nie, Z.; Chen, X.; Wang, C.; Liu, J. A Facile Approach using $MgCl_2$ to Formulate High Performance Mg^{2+} Electrolytes for Rechargeable Mg Batteries. *J. Mater. Chem. A*, **2014**, *2*, 3430-3438.

13. Barile, C.; Spatney, R.; Zavadil, K.; Gewirth, A. Investigating the Reversibility of in Situ Generated Magnesium Organohaloaluminates for Magnesium Deposition and Dissolution. *J. Phys. Chem. C*, **2014**, *118*, 10694-10699.

14. Shterenberg, I.; Salama, M.; Gofer, Y.; Levi, E.; Aurbach, D. The Challenge of Developing Rechargeable Magnesium Batteries. *MRS Bull.*, **2014**, *39*, 453-460.

15. Williams, D.; Lawton, M. Drying of Organic Solvents: Quantitative Evaluation of the Efficiency of Several Dessicants. *J. Org. Chem.*, **2010**, *75*, 8351-8354.

16. Benmayza, A.; Ramanathan, M.; Arthur, T.; Matsui, M.; Mizuno, F.; Guo, J.; Glans, P.; Prakash, J. Effect of Electrolyte Properties of a Magnesium Organohaloaluminate Electrolyte on Magnesium Deposition. *J. Phys. Chem. C*, **2013**, *117*, 26881-26888.

17. Meerwein, H.; Delfs, D.; Morschel, H. Die Polymerisation des Tetrahydrofurans. *Angew. Chem.*, **1960**, *72*, 927-934.

18. Zhang, W.; Hu, J.; Ding, X.; Wu, Y.; Ye, Z. Synthesis and Crystal Structure of $[Mg_3Cl_5(Et_2O)_6]^+[Me_2SbI_2]^-$. *Inorg. Chem. Commun.*, **2003**, *6*, 1185-1187.

19. Pirinen, S.; Koshevoy, I.; Denifl, P.; Pakkanen, T. A Single-Crystal Model for $MgCl_2$–Electron Donor Support Materials: $[Mg_3Cl_5(THF)_4Bu]_2$ (Bu = *n*-Butyl). *Organometallics*, **2013**, *32*, 4208-4213.

20. Eckert, J.; Galova, M. Electrode Kinetics of the Aluminum Deposition from Tetrahydrofuran Electrolytes. *Electrochim. Acta.*, **1981**, *26*, 1169-1175.

21. Schwarzenbach, G. Der Chelateffekt. *Helv. Chim. Acta.*, **1952**, *35*, 2344-2359.